THE ASTROPHYSICAL JOURNAL SUPPLEMENT SERIES, 68:257–286, 1988 October

A CATALOG OF SMALL, OPTICALLY SELECTED MOLECULAR CLOUDS: OPTICAL, INFRARED, AND MILLIMETER PROPERTIES

DAN P. CLEMENS[1,2]
Steward Observatory, University of Arizona
AND
RICHARD BARVAINIS[1]
National Radio Astronomy Observatory, Charlottesville, Virginia
Received 1987 July 14; accepted 1988 January 18

ABSTRACT

A catalog of 248 small molecular clouds selected from the northern hemisphere Palomar Observatory Sky Survey is presented. These clouds have angular sizes of less than 10′ (the mean of the sample is 4′), are reasonably well isolated, and are centrally opaque. They most closely resemble small versions of the larger Bok globules and Barnard objects. Many (30%) of the smallest members of this catalog have not been previously cataloged or studied. Coordinates accurate to 0.5, optical extents and orientation angles, and cross references are given for all of the clouds. Radial velocities, obtained from CO observations, are listed for 242 of the clouds. Additionally, 346 associated or possibly associated *IRAS* point sources are listed for 149 of the clouds. Since most of these clouds have few or no foreground stars and subtend small angular extents, they are likely the smallest (all <1.5 pc) and simplest dark molecular clouds in the Galaxy. The mean ellipticity (a/b) of the clouds in the catalog is 2.0, indicating that spherical cloud models may not be appropriate for this sample. The mean orientations, with respect to the Galactic plane, of the clouds showing ellipticities greater than unity has no angular dependence; that is, the local Galactic plane does not seem to order the direction of the optically determined ellipticity for the clouds.

The far-infrared properties of the clouds with associated *IRAS* sources are similar to those seen in the sample of dark cloud cores studied by Beichman and coworkers, but are somewhat cooler (19 K versus 28 K for the mean dust temperatures derived from 60–100 μm flux ratios) and less FIR–bright. Millimeter ^{12}CO $J = 2$–1 observations of the centers of 93 of the cataloged clouds shows that most (70%) of the sample are cool (gas kinetic temperature ~ 8 K) and quiescent (gasdynamical motions approximately sonic). Some clouds exhibit warmer gas temperatures possibly driven by radiative heating from nearby stars. Another small group of clouds exhibits the cool temperatures and supersonic line widths characteristic of possible embedded protostellar activity.

Subject headings: infrared: sources — interstellar: molecules — nebulae: general — radial velocities

I. INTRODUCTION

What is the physical nature of molecular gas prior to the formation of stars, and what processes play important roles in exciting star formation? These questions are extremely important, and yet studies of Orion and other high-mass star formation regions can provide few answers because the new stars have destroyed much of the evidence sought. An understanding of the cloud's molecular gas and dust *earlier* in the star-forming history of the cloud is needed. Hence, a collection of clouds is required which either have not yet formed stars or have only very recently formed low-mass stars.

Furthermore, the clouds should have simple structures. Supersonic line widths, local H II regions, or associated large molecular clouds or complexes will likely affect the regions of interest. The clouds should be nearby, so that linear scales of the order of tenths or hundredths of parsecs may be resolved. Finally, the clouds should be small to ensure their simplicity and so that current instruments (single-dish millimeter-wave telescopes and optical and infrared CCDs) can completely sample them in a small number of observing sessions.

Such a catalog of small molecular clouds was needed for our ongoing study of star formation in Bok globules (Clemens and Leach 1987; Clemens, Leach, and Barvainis 1988). The available catalogs (Lynds 1962; Barnard 1927) are most complete for larger clouds (i.e., angular sizes greater than 5′–10′). However, many smaller clouds do not appear in these catalogs. A new search of the Palomar Observatory Sky Survey (POSS) was made with the goal of finding the smaller molecular clouds.

We have identified 248 molecular clouds with optical sizes smaller than 10′. Most of these have been previously cataloged (72%), although the fraction of clouds previously cataloged decreases somewhat (to 60%) as the mean size decreases to 1′–2′. A large number of the clouds (60%) have *IRAS* point sources within their boundaries or in their near environs, indicating that probing the FIR dust properties of the clouds will be productive.

In the following section the selection criteria used in the search and to create the catalog are described. Section III

[1] Guest Observer, Five College Radio Astronomy Observatory, University of Massachusetts, New Salem, Massachusetts.
[2] Guest Observer, Millimeter Wave Observatory, University of Texas, Fort Davis, Texas.

presents the catalog and the associated *IRAS* sources and millimeter-wave observations. In § IV the optical, infrared, and radio properties are summarized for the cloud sample and correlated between the wavelengths.

II. SELECTION CRITERIA AND CATALOG

Since a catalog of Bok globule–like objects was sought, our search was aimed at finding the clouds with the smallest angular extents, showing optically opaque cores and good isolation from connecting interstellar material. Roundness and ellipticity were specifically *not* selection criteria, since the shape of a cloud may depend on its rotational evolution or magnetic field properties—properties that we wish to probe with this sample of clouds. As a result, the catalog has a large range of ellipticities (a/b up to 7).

Every POSS plate (both O and E) between $\delta = 90°$ and $\delta = -36°$ was examined for the presence of small, opaque clouds. Those clouds which were smaller than 10′ (mean size) and reasonably free from connecting material were selected for the catalog. A small bias in our search toward isolated clouds tended to select against clouds in regions with nearby, larger cloud complexes. Clouds with multiple opaque cores or long, stringy filaments were also generally excluded, though the B72 complex was included. In order to obtain a sample of clouds from very different environments, an effort was made to both avoid other well-studied regions (e.g., Ophiuchus, Taurus, and Orion; see § IV*b* below), and to not draw too many clouds for the catalog from any one region of the sky.

The sizes of the fully opaque cores were generally measured on the POSS O plate (blue), although the E plates were measured for sources in regions showing high extinction in the blue (especially for Galactic longitudes between 0° and 30°). The true shapes of the clouds were approximated by ellipses and the major and minor axes and position angles were measured by hand. The sizes were originally measured to the nearest millimeter (~ 67″); hence, while the catalog lists sizes in arcminutes to one decimal place, the precision is not that high. For objects with large ellipticities ($a/b \geq 1.5$), the position angles are accurate to about 20°. The center coordinates were estimated by eye and for round objects are accurate to 0.5. For more extended or complex shaped objects the notion of a center breaks down and the coordinates listed serve only to identify the cloud as being distinct from some other nearby condensation.

III. THE CATALOG

Table 1 lists the 248 cloud entries and their associated *IRAS Point Source Catalog* (1985, hereafter PSC) (version 2) detections. Column (1) contains the right ascension-ordered identifying number for each cloud. Columns (2) and (3) list the central 1950.0 right ascension and declination. Columns (10) and (11) show the Galactic coordinates. Column (4) indicates the CO millimeter-wave velocity, where available. The references for the velocities are indicated in the comments. Columns (5), (6), and (7) list the optical data obtained from the POSS prints, namely, major-axis diameter, minor-axis diameter, and position angle of the major axis (measured east from north). Column (8) lists other cataloged names for the 178 clouds with other associations. In that column KHAV refers to Khavtassi (1955), L to Lynds (1962), LBN to Lynds (1965), B to Barnard (1927), DC to Dickman and Clemens (1983), SCHO to Schoenberg (1964), and MBM to Magnani, Blitz, and Mundy (1985).

Column (9) contains comments on the optical appearance and radial velocity reference. In that column, R refers to the presence of nebulosity on the POSS O plate, i.e., a reflection nebula; H refers to nebulosity on the E plate, hence Hα nebulosity; B refers to bright rims of both reflection and Hα; E indicates that the POSS E plate was the source of the optical measurements; and C signals that the isolation of the cloud from neighboring material is significantly worse than average (i.e., the cloud is "connected").

a) *Correlation with IRAS Point Source Catalog*

The cataloged optical sizes and orientations were used to define "core," "envelope," and "reference" regions for each cloud. The core region was chosen to be identical to the cataloged optical size and orientation, the envelope region to have twice the semimajor and semiminor axes as the core region (but not to include the core region), and the reference region to have twice the axes of the envelope region (and, again, not to include the previous two regions). Thus the areas of the three regions are in the ratio of 1:3:12. Every *IRAS* PSC source (from the second release of the PSC) that fell into each of the three regions for each cloud was found, and the *IRAS* fluxes and source names appear in columns (12), (13), (14), (15), (16), and (17) of Table 1.

Columns (12), (13), (14), (15), (16), and (17) report the 12, 25, 60, and 100 μm fluxes, names, and locations in the clouds of any *IRAS* point source associated with either the core or the envelope region of each cloud. As in the printed version of the PSC, the characters following each flux value indicate the quality of the flux measurement—A is a high-quality value, B is a lower quality value, and U indicates an upper limit. The PSC name is in the usual *HHMMM* ± *DDMM* format.

The *IRAS* sources for each cloud are listed as core sources first, followed by envelope sources. The number of *IRAS* sources falling in the reference region for each cloud was used to estimate the likelihood of the core and envelope sources appearing by chance. The numbers in column (17) following the first core and envelope source listed for each cloud indicate the chance association probability. That number represents the number of chance sources that should appear in the indicated region. For example, the listing for cloud 97 in Table 1 has two core sources and three envelope sources listed. The first core source line also lists the chance association number for the core, as derived from the number of sources in the reference region. The value of 0.7 indicates that, of the two core sources listed, one is likely there by chance, most likely due to background or foreground sources superposed on the sky with the opaque core. In fact, *both* core sources have 12 μm fluxes that are greater than their 25 μm fluxes, and are therefore probably stars. Similarly, the envelope sources should have about two sources that are there by chance. For this cloud, one of the envelope sources is seen only at 12 μm (again likely a star), while the other two sources have 60 or 100 μm detections, indicating objects much cooler than stars. As shown in § IV*c* below, the chance probability tabulated for the core regions is an upper limit (by

TABLE 1

SMALL CLOUD CATALOG

No. (1)	α_{1950} (2)	δ_{1950} (3)	V_{LSR} (4)	a (5)	b (6)	P.A. (7)	Other Names (8)	Comments (9)
	ℓ (10)	b (11)	$S_{12\mu m}$ (12)	$S_{25\mu m}$ (13)	$S_{60\mu m}$ (14)	$S_{100\mu m}$ (15)	PSC No. (16)	Location (17)
1	$0^h12^m00^s$	63°53′00″	−3.2	2.2	2.2	0	KHAV3	a
	119.0872	1.3475						
2	$0^h16^m20^s$	63°38′52″	−2.4	3.4	3.4	0	L1281	a
	119.3842	1.2770						
3	$0^h26^m00^s$	56°25′33″	−38.3	6.7	5.6	45	LBN594	a
	119.8062	−6.0317	.76A	1.12A	30.56A	108.50B	00259+5625	Core .0
4	$0^h36^m15^s$	52°35′00″	−11.3	2.2	1.1	45	DC	b, B
	121.0362	−9.9682	.25U	.25U	.40U	5.04A	00362+5234	Core .0
5	$0^h41^m09^s$	62°13′37″	4.1	4.5	3.4	0	L1301	b
	122.0868	−.3591						
6	$0^h46^m38^s$	50°28′21″	−12.5	9.0	3.4	−50	LBN613	a, C, B
	122.6173	−12.1256	.25U	1.01A	3.96A	8.96A	00465+5028	Core .3
7	$1^h09^m00^s$	64°10′00″	0.1	6.7	5.6	−45		b
	125.1774	1.6511	.29U	.25U	.75A	18.64U	01087+6404	Envl .3
8	$1^h20^m00^s$	74°06′52″	2.2	7.8	5.6	40		b,H
	125.1598	11.6445	.25U	.85U	.40U	7.41A	01202+7406	Core .0
9	$1^h26^m29^s$	62°50′00″	2.7	6.7	4.5	−50	L1325	b
	127.2655	.5436						
10	$1^h27^m16^s$	67°08′19″	0.5	9.0	5.6	20		b
	126.7153	4.8145						
11	$1^h33^m31^s$	64°47′26″	−1.9	10.1	4.5	−20		b
	127.7216	2.5986	.38U	.34A	1.94A	3.20U	01333+6448	Core .3
			.25U	.51U	.53B	6.38A	01334+6442	Core
12	$1^h35^m05^s$	64°50′00″	−11.4	9.0	7.8	0		b
	127.8779	2.6696	.25U	.25U	.60A	7.88B	01354+6447	Core .1
13	$1^h53^m19^s$	62°26′40″	−35.9	4.5	2.2	20	L1345	a
	130.3626	.7654						
14	$1^h54^m00^s$	62°25′00″	−11.0	4.5	3.4	45	L1346	a
	130.4455	.7577						
15	$3^h52^m38^s$	55°59′21″	0.8	11.2	7.8	45	B6,L1387	a
	146.7032	2.0596	.26U	.66U	.52U	5.79A	03521+5555	Core .2
			.27U	.29U	1.00A	2.34U	03523+5608	Envl .5
16	$3^h59^m16^s$	56°41′52″	−2.2	6.7	2.2	−80	L1388	a
	146.9459	3.1950	.25U	.25U	.40U	3.96A	03592+5642	Core .1
17	$4^h00^m35^s$	56°48′00″	−4.7	2.2	2.2	60	L1389	a
	147.0158	3.3915	.45U	.25U	.91A	5.78A	04005+5647	Core .0
18	$4^h00^m44^s$	60°24′09″	−2.9	2.2	1.1	50		a, C
	144.6399	6.1071						
19	$4^h23^m42^s$	25°31′40″	6.6	7.8	5.6	0		a
	172.1534	−16.0351	.25U	.65U	.40U	2.33A	04233+2529	Envl .3
			1.00A	1.21A	.69A	2.08U	04240+2535	Envl

TABLE 1—*Continued*

No. (1)	α_{1950} (2)	δ_{1950} (3)	V_{LSR} (4)	a (5)	b (6)	P.A. (7)	Other Names (8)	Comments (9)
	ℓ (10)	b (11)	$S_{12\mu m}$ (12)	$S_{25\mu m}$ (13)	$S_{60\mu m}$ (14)	$S_{100\mu m}$ (15)	PSC No. (16)	Location (17)
20	$4^h33^m09^s$	24°37′12″	5.7	4.5	1.1	80	L1533(?)	a
	174.3248	−15.0184						
21	$4^h37^m00^s$	29°40′00″	6.8	4.5	2.2	45		a, C
	170.9541	−11.0917						
22	$4^h37^m25^s$	29°48′57″	2.5	6.7	2.2	−40	B23,L1503	a, E
	170.9006	−10.9236						
23	$4^h40^m22^s$	29°34′26″	5.6	5.6	3.4	50	L1507(?)	b
	171.5093	−10.5936						
24	$4^h54^m33^s$	52°11′07″	4.6	2.2	2.2	0		a
	155.7601	5.9068						
25	$4^h55^m08^s$	51°58′52″	5.2	2.2	2.2	0	L1437	a
	155.9760	5.8495						
26	$4^h56^m13^s$	52°00′33″	5.8	6.7	3.4	90	L1439	b
	156.0584	5.9987	.27U	.32U	4.88A	11.08A	04559+5200	Core .2
27	$5^h01^m00^s$	32°43′21″	6.9	10.1	5.6	20	SCHO93	a
	171.8229	−5.1821	.64A	.31U	.40U	5.55U	05013+3234	Envl .8
28	$5^h03^m51^s$	−04°00′00″	8.8	4.5	4.5	0	LBN923	a, B
	204.0172	−25.1085	.25U	.26U	1.11A	21.35U	05036-0359	Core .1
			.27U	.26U	1.32A	1.51U	05037-0402	Core
			.25U	.25U	.82U	16.39A	05038-0400	Core
29	$5^h19^m42^s$	−03°44′24″	11.2	6.7	4.5	60		b, B
	205.8061	−21.5012	.43U	.27U	2.26A	30.54U	05194-0346	Core .0
			.40U	.32U	2.72A	31.80U	05194-0343	Core
			.78U	.55U	.74A	7.03U	05190-0348	Envl .0
			.25U	.25U	1.16B	7.84A	05201-0341	Envl
30	$5^h27^m04^s$	05°42′45″	−0.1	7.8	4.5	20		b, C, H
	198.0669	−15.2657	.25U	.25U	1.54A	12.08A	05268+0538	Core .4
			.56A	.26U	1.66U	9.75U	05268+0550	Envl 1.3
			.25U	.25U	.49B	8.26A	05274+0542	Envl
31	$5^h30^m48^s$	−00°40′00″	−7.2	5.6	3.4	−30	IC423,LBN913	b, B
	202.9570	−16.8765	.25U	.58A	2.64U	30.66U	05307-0038	Core .2
32	$5^h33^m55^s$	−00°18′25″	−5.1	5.6	3.4	90	IC426,LBN921	b, B
	203.7985	−16.4331	1.09A	1.47A	1.55U	35.15B	05337-0019	Core .1
			.25U	.26U	1.08A	26.48U	05344-0016	Envl .3
33	$5^h43^m38^s$	20°44′26″	0.8	5.6	3.4	10		b
	187.1139	−4.0496	.79U	.67U	.40U	3.28A	05437+2045	Core .0
			1.58A	.37A	.44U	1.86U	05433+2040	Envl .0
34	$5^h44^m02^s$	21°00′07″	0.7	4.5	2.2	90		b
	186.9389	−3.8338	.88A	2.78A	10.68A	28.66A	05440+2059	Core .1
35	$5^h44^m27^s$	10°25′33″	9.4	4.5	2.2	90		b, C
	196.1324	−9.1714						
36	$5^h50^m06^s$	17°06′07″	1.1	3.4	1.1	−45		b
	191.0689	−4.5459						

TABLE 1—*Continued*

No. (1)	α_{1950} (2)	δ_{1950} (3)	V_{LSR} (4)	a (5)	b (6)	P.A. (7)	Other Names (8)	Comments (9)
	ℓ (10)	b (11)	$S_{12\mu m}$ (12)	$S_{25\mu m}$ (13)	$S_{60\mu m}$ (14)	$S_{100\mu m}$ (15)	PSC No. (16)	Location (17)
37	$5^h57^m24^s$	31°39′26″	1.2	5.6	4.5	90	L1555	b, C
	179.2985	4.1781						
38	$5^h58^m02^s$	16°56′48″	3.1	2.2	1.1	90		a
	192.1235	−3.0450						
39	$5^h59^m05^s$	16°30′28″	2.4	4.5	3.4	0		b, R
	192.6304	−3.0444	4.53A	9.86A	7.27A	10.64A	05591+1630	Core .2
40	$5^h59^m12^s$	16°41′06″	2.8	5.6	2.2	0		b
	192.4902	−2.9322	.34U	.29U	.88A	3.54U	05592+1640	Core .1
			.71A	.27B	.40U	3.40U	05589+1638	Envl .3
41	$5^h59^m38^s$	16°29′55″	2.9	5.6	2.2	0		b
	192.7034	−2.9357						
42	$5^h59^m48^s$	16°40′00″	2.8	6.7	2.2	70		a
	192.5759	−2.8200	.39U	.45B	.97A	3.96U	06000+1644	Envl .5
43	$6^h00^m18^s$	16°37′14″	3.3	4.5	3.4	−50		a, C
	192.6758	−2.7377						
44	$6^h04^m34^s$	19°28′19″	−0.5	9.0	5.6	−15	B227,L1570	b, C
	190.6953	−.4479	.25U	.52A	.61A	12.84U	06047+1923	Core .0
			.26U	.42U	1.57A	18.95U	06048+1934	Envl .0
45	$6^h06^m00^s$	17°50′52″	0.8	10.1	7.8	−35	L1578(?)	b, C
	192.2761	−.9501	.37A	.32U	.51U	5.59U	06055+1800	Envl 1.3
46	$6^h17^m09^s$	07°06′07″	19.5	4.5	1.1	85		a
	203.0166	−3.7317						
47	$6^h17^m15^s$	07°09′33″	19.3	2.2	2.2	0		a
	202.9774	−3.6833						
48	$6^h17^m36^s$	07°11′42″	18.6	3.4	1.1	0		a
	202.9855	−3.5923	.95U	.30U	.40U	2.61A	06175+0711	Core .0
49	$6^h22^m05^s$	03°23′52″	9.6	4.5	3.4	45	L1633	a, C
	206.8721	−4.3896						
50	$6^h31^m39^s$	07°50′00″	0.9	3.4	2.2	−40		a, R
	204.0564	−.2152	.26U	.35U	3.04A	18.10B	06316+0748	Core .1
51	$6^h35^m15^s$	01°34′26″	...	3.4	2.2	10	LBN978	H, C
	210.0196	−2.3233	.25U	.28A	2.32B	6.26B	06355+0134	Envl .0
52	$6^h46^m29^s$	−16°50′00″	16.6	6.7	3.4	−65		a
	227.7676	−8.1947	.61A	.80A	9.53A	38.41A	06464-1650	Core .0
			1.43U	.25U	.43U	2.54A	06459-1646	Envl .0
			.56A	1.27A	.76A	1.55U	06464-1644	Envl
			.25U	.25U	.40U	3.38A	06471-1651	Envl
53	$6^h48^m58^s$	05°16′40″	...	2.2	2.2	0		
	208.3083	2.4205	5.89A	1.93A	.54U	7.18U	06487+0517	Envl .3
54	$7^h02^m02^s$	−16°20′00″	19.5	5.6	3.4	40	LBN1042	a
	229.0033	−4.6445	.57A	3.66A	43.34A	111.50A	07020-1618	Core .1
			.32A	.25U	.40U	1.88U	07023-1621	Envl .3

TABLE 1—*Continued*

No. (1)	α_{1950} (2)	δ_{1950} (3)	V_{LSR} (4)	a (5)	b (6)	P.A. (7)	Other Names (8)	Comments (9)
	ℓ (10)	b (11)	$S_{12\mu m}$ (12)	$S_{25\mu m}$ (13)	$S_{60\mu m}$ (14)	$S_{100\mu m}$ (15)	PSC No. (16)	Location (17)
55	$7^h02^m30^s$	−16°31′07″	20.0	7.8	1.1	80		b
	229.2194	−4.6310	.25U	.25U	.40U	3.19A	07025-1631	Core .0
			20.67A	11.00A	2.23A	1.72U	07019-1631	Envl .0
56	$7^h12^m32^s$	−25°03′38″	14.5	4.5	2.2	−10		b, B
	237.9274	−6.4587	.25U	.23B	1.18A	10.54B	07125-2503	Core .0
			1.63A	.29A	.40U	9.43U	07125-2507	Envl .0
57	$7^h15^m27^s$	−22°56′07″	20.3	5.6	2.2	−20		b
	236.3430	−4.8846	.25U	.25U	.97A	7.11A	07156-2301	Envl .5
58	$7^h16^m07^s$	−23°33′21″	15.0	7.8	3.4	−10		b, H
	236.9655	−5.0388	.25U	.27U	2.21U	9.59A	07159-2329	Core .1
			.25U	.27B	3.34A	14.11B	07161-2336	Core
			.29A	.25U	1.60U	20.68U	07163-2328	Envl .3
59	$7^h16^m53^s$	04°02′26″	10.6	5.6	3.4	−55		a
	212.6043	8.0436	.25U	.25U	.40U	2.87A	07171+0359	Core .1
60	$8^h02^m37^s$	−31°22′12″	13.9	10.1	6.7	40	L1670	b, R
	248.8908	−.0110	1.64A	2.39A	19.73A	67.04B	08026-3122	Core .4
			.50U	.25U	.55A	12.76U	08029-3118	Core
			.25U	.30A	.42B	8.05U	08022-3115	Envl 1.3
61	$11^h30^m34^s$	79°47′14″	...	11.2	6.7	−55		
	127.2695	36.9555						
62	$13^h29^m47^s$	79°38′00″	...	3.4	2.2	0		
	120.6958	37.5840						
63	$15^h48^m11^s$	−03°57′14″	2.5	11.2	6.7	−90	LBN11	a, H
	4.1641	36.6390	.25U	.27U	.40U	2.53A	15486-0350	Envl 1.0
64	$15^h57^m35^s$	−01°18′19″	0.5	4.5	2.2	30	LBN37	a, B, E
	8.5576	36.3817						
65	$16^h28^m18^s$	−23°34′57″	2.3	10.1	3.4	80	L1704	a, E
	354.3958	16.5338	.74U	.54U	.92A	20.02U	16277-2332	Envl .5
			2.70A	1.13A	.42U	24.42U	16287-2337	Envl
66	$16^h36^m41^s$	−14°00′00″	3.4	13.4	3.4	45	L121,MBM142	b
	3.5812	21.0272	.25U	.38U	.40U	4.21A	16371-1353	Core .2
67	$16^h47^m38^s$	−19°02′45″	4.6	15.7	3.4	−70	L31	a
	.9423	15.9798	.65A	.36U	.46U	10.57U	16482-1906	Core .1
			.47U	.43U	.42U	3.82A	16485-1906	Envl .3
68	$16^h54^m24^s$	−16°04′45″	5.0	4.5	3.4	0	L146(?)	a, C
	4.4977	16.3511	.25U	1.48A	19.46A	33.65A	16544-1604	Core .1
69	$16^h59^m26^s$	−33°12′45″	18.5	10.1	4.5	−60	B49	b
	351.2334	5.1419	2.71A	2.92A	.88U	10.02U	16594-3315	Core .9
			1.61A	1.49A	1.44U	26.75A	16595-3311	Core
			.77A	.50U	.84U	9.09U	16586-3304	Envl 2.8
			59.41A	58.83A	9.24A	7.03U	16589-3315	Envl
			.80B	1.30A	1.75U	8.82U	16590-3313	Envl
			.55A	1.70A	5.29A	6.75U	16590-3305	Envl

TABLE 1—*Continued*

No. (1)	α_{1950} (2)	δ_{1950} (3)	V_{LSR} (4)	a (5)	b (6)	P.A. (7)	Other Names (8)	Comments (9)
	ℓ (10)	b (11)	$S_{12\mu m}$ (12)	$S_{25\mu m}$ (13)	$S_{60\mu m}$ (14)	$S_{100\mu m}$ (15)	PSC No. (16)	Location (17)
70	$17^h00^m00^s$	−22°09′26″	2.6	9.0	3.4	80	L4	b
	.2309	11.7079	.52A	.33U	.40U	5.71A	16598-2208	Core .2
71	$17^h02^m10^s$	−22°08′52″	2.9	7.8	3.4	−30		a, E, C
	.5407	11.3083	.25U	.28U	.79A	8.41U	17021-2203	Core .6
72	$17^h05^m29^s$	−22°50′00″	4.7	9.0	5.6	−20	B57,L11	a, C
	.4346	10.2829	.59A	.65U	.41U	11.07U	17051-2257	Envl 1.0
			.29U	.34U	1.28A	4.14U	17054-2302	Envl
73	$17^h05^m33^s$	−32°03′05″	13.8	4.5	3.4	50	B56,L1685	a, C
	352.9429	4.8183	.42A	.44U	2.81U	16.70A	17056-3204	Core .2
			2.33A	1.32A	3.53U	35.67U	17052-3207	Envl .5
			.57A	.41U	2.76U	32.82U	17059-3159	Envl
74	$17^h08^m48^s$	−22°25′00″	3.8	7.8	5.6	50	B60,L38(?)	a, E, C
	1.2300	9.9025	.25U	.89U	.40U	7.35A	17085-2225	Core .4
75	$17^h09^m52^s$	−30°12′12″	9.5	4.5	2.2	−65	B247	a, E
	354.9858	5.1701	.30U	.39U	1.67A	15.30A	17099-3012	Core .1
76	$17^h12^m04^s$	−20°26′38″	1.2	11.2	3.4	60	B61,L111	b
	3.3152	10.4086	.25U	.33U	.40U	7.13A	17119-2027	Core .2
			.99A	.35U	.44U	3.78U	17113-2033	Envl .5
			39.06A	22.53A	2.75A	3.06U	17122-2019	Envl
			.53A	.62U	.41U	5.35U	17128-2024	Envl
77	$17^h12^m39^s$	−01°40′00″	−0.3	6.7	4.5	0		a
	19.8301	20.4108						
78	$17^h14^m23^s$	−18°28′21″	4.3	10.1	5.6	−10	B64,L173	b, C
	5.2855	11.0697	.25U	.32U	.40U	3.67A	17147-1821	Envl .8
79	$17^h16^m37^s$	−26°40′00″	3.6	12.3	4.5	50	B65,L1772	a, E, C
	358.7468	6.0074	.35U	.34U	.86A	8.88U	17166-2648	Envl 2.8
			.49A	.42U	.68U	9.57U	17174-2630	Envl
80	$17^h18^m50^s$	−21°45′31″	2.4	1.1	1.1	0	L101	b
	3.1155	8.3653						
81	$17^h19^m30^s$	−27°02′12″	3.4	11.2	5.6	90	L1774	a, E
	358.8074	5.2691	.72U	6.19A	6.73A	10.89U	17193-2705	Core 1.3
			6.84B	20.34A	10.34B	11.02U	17195-2710	Envl 3.8
			.71A	.39U	.95U	11.97U	17204-2659	Envl
82	$17^h19^m34^s$	−23°47′45″	3.4	4.5	3.4	20	B68,L55	b
	1.5093	7.0822	6.11A	2.71A	.59U	16.85U	17194-2351	Core .1
83	$17^h20^m00^s$	−23°31′03″	5.0	10.1	3.4	45	B72,L66(?)	a, C
	1.7982	7.1555						
84	$17^h20^m30^s$	−23°37′45″	4.7	4.5	3.4	−45	B72,L66(?)	a, C
	1.7680	7.0003						
85	$17^h20^m57^s$	−23°39′26″	5.0	5.6	3.4	−45	B72,L66(?)	b, C
	1.8024	6.8996	.50U	.37U	1.14A	21.83U	17214-2340	Envl .8
86	$17^h21^m48^s$	−23°33′17″	4.4	10.1	3.4	−60	B72,L66(?)	b, C
	1.9982	6.7945	.26U	.39U	.61U	10.07A	17219-2333	Core .4

TABLE 1—*Continued*

No. (1)	α_{1950} (2)	δ_{1950} (3)	V_{LSR} (4)	a (5)	b (6)	P.A. (7)	Other Names (8)	Comments (9)
	ℓ (10)	b (11)	$S_{12\mu m}$ (12)	$S_{25\mu m}$ (13)	$S_{60\mu m}$ (14)	$S_{100\mu m}$ (15)	PSC No. (16)	Location (17)
			.50A	.51U	.67U	18.65U	17218-2339	Envl 1.3
			.55A	.35U	.72U	7.69U	17224-2334	Envl
87	$17^h22^m00^s$	−24°10′00″	4.7	9.0	9.0	0	B74	a, C
	1.5119	6.4163	.46U	.50U	1.33A	17.17U	17217-2409	Core 1.0
			.28U	.36U	.79A	17.17U	17217-2404	Core
			.25U	.29U	.54U	17.17A	17220-2410	Core
			1.48A	.37U	1.34B	29.23U	17220-2412	Core
			.35A	.39U	.69U	35.01U	17222-2414	Core
			.39U	.44U	.80B	10.34A	17222-2404	Core
			.30U	.41U	1.88A	26.70U	17224-2410	Core
			.84A	.55U	.67U	25.75U	17211-2413	Envl 3.0
			.65A	.73A	.61U	25.56U	17212-2407	Envl
			.66A	.44U	.62U	40.39U	17223-2422	Envl
			.57A	.91U	1.25U	40.18U	17225-2406	Envl
			2.64A	1.77A	.55U	24.36U	17226-2359	Envl
			.26U	.34U	1.07U	12.51A	17228-2408	Envl
88	$17^h25^m35^s$	−25°13′52″	3.6	7.8	4.5	−50	B267,L36	a
	1.0769	5.1478	.35U	.51U	1.89A	33.77U	17256-2516	Core .6
			.73A	.37U	.72U	41.91U	17258-2510	Envl 1.8
			.39U	.47U	1.45A	33.79U	17259-2517	Envl
89	$17^h29^m09^s$	−25°23′21″	3.8	5.6	2.2	75	L52	b, E
	1.3915	4.3851	1.11A	1.13A	2.97U	35.82U	17287-2526	Envl .8
90	$17^h35^m29^s$	−19°42′50″	10.4	2.2	1.1	50	L216(?)	a, E, C
	6.9830	6.2144						
91	$17^h36^m36^s$	−19°35′00″	10.5	4.5	3.4	−35	L219	b, E, C
	7.2337	6.0620	.45B	.63A	1.05A	19.36U	17366-1934	Core .2
			.49A	.85U	.63U	20.81U	17363-1937	Envl .5
			.78A	.46A	.44U	24.37U	17365-1930	Envl
			.86A	.51B	.66U	22.27U	17366-1928	Envl
92	$17^h37^m47^s$	−19°38′21″	10.5	4.5	2.2	−40	L226	a, E
	7.3345	5.7949	.64A	.40U	.55U	19.61U	17375-1936	Envl .8
			1.11A	.65U	.52U	29.32U	17376-1934	Envl
			.37U	.50U	.99U	5.67A	17380-1937	Envl
93	$17^h37^m52^s$	−19°42′50″	10.3	2.2	1.1	0	L223	b, E
	7.2807	5.7396						
94	$17^h38^m25^s$	−19°46′11″	10.6	2.2	1.1	0	L222	b, E
	7.3020	5.5991						
95	$17^h42^m23^s$	−19°59′20″	11.1	3.4	1.1	30	B83, L233	b
	7.6044	4.6910						
96	$17^h43^m25^s$	−20°04′56″	10.8	2.2	2.2	0	L235	b, E
	7.6512	4.4356						
97	$17^h43^m49^s$	−20°15′33″	10.5	6.7	3.4	55	B84,L235	b, E, C
	7.5481	4.2639	.78A	.66U	1.00U	13.27U	17438-2015	Core .7
			2.48A	1.49A	.74U	10.35U	17438-2017	Core
			.51A	.40U	1.10U	12.78U	17432-2020	Envl 2.0

TABLE 1—*Continued*

No. (1)	α_{1950} (2)	δ_{1950} (3)	V_{LSR} (4)	a (5)	b (6)	P.A. (7)	Other Names (8)	Comments (9)
	ℓ (10)	b (11)	$S_{12\mu m}$ (12)	$S_{25\mu m}$ (13)	$S_{60\mu m}$ (14)	$S_{100\mu m}$ (15)	PSC No. (16)	Location (17)
			1.27U	.35U	1.21A	10.85A	17434-2014	Envl
			2.94U	.39U	1.14A	13.68U	17438-2019	Envl
98	$17^h44^m02^s$	−20°29′26″	10.7	3.4	2.2	−60		b, E
	7.3770	4.0992						
99	$17^h44^m05^s$	−20°16′40″	10.6	2.2	1.1	−30	L235	b, E
	7.5661	4.1984						
100	$17^h49^m08^s$	−02°58′07″	4.6	9.0	4.5	−60		a
	23.3160	11.8344	.53U	.28U	.40U	4.96A	17490-0258	Core .3
			.25U	.25U	.40U	4.60A	17493-0258	Core
101	$17^h50^m33^s$	−08°24′26″	6.7	12.3	4.5	25	L392	b
	18.6634	8.8747	.42A	.28U	.42U	3.98U	17503-0833	Core .2
			1.60A	.73A	.40U	7.69A	17505-0828	Core
102	$17^h51^m34^s$	−27°49′26″	8.3	9.0	3.4	85		b
	1.9753	−1.1534	9.01A	12.64A	27.74U	266.90U	17515-2747	Core 1.6
			2.17U	3.43U	15.48U	164.10A	17508-2750	Envl 4.8
			1.63A	2.80U	17.68U	406.30U	17512-2754	Envl
			2.24A	2.35B	12.87U	68.58B	17513-2745	Envl
			2.99U	1.31A	27.98U	353.30U	17514-2752	Envl
			1.60A	1.46A	19.68U	360.70U	17520-2752	Envl
			1.90A	3.40U	26.57U	399.40U	17522-2744	Envl
103	$17^h52^m48^s$	−02°48′19″	6.0	7.8	4.5	−60		b
	23.9106	11.1105						
104	$17^h52^m48^s$	−08°15′00″	10.6	9.0	4.5	90	L400	b, E
	19.0804	8.4662	.25U	.30U	.40U	4.60A	17526-0815	Core .2
			.55A	.34U	.40U	17.14U	17533-0808	Envl .5
105	$17^h55^m28^s$	−03°46′07″	6.7	7.8	4.5	−55	L460	b, E
	23.3751	10.0651	.36U	.76U	.40U	3.81A	17561-0349	Envl .8
106	$17^h57^m57^s$	−03°30′33″	6.2	11.2	5.6	−60	L468	a, E
	23.9077	9.6451	.25U	.25U	.40U	4.85A	17577-0329	Core .3
			.32U	.52U	.61U	4.49A	17580-0330	Core
			.25U	.60U	.40U	3.04A	17586-0330	Envl 1.0
107	$17^h59^m49^s$	−27°52′14″	11.6	4.5	3.4	30	B86,L93	b, H
	2.8528	−2.7538	1.66A	1.30B	14.42U	268.90U	17597-2754	Core .5
			4.33A	1.12A	15.21U	205.10U	17597-2749	Core
			4.88A	4.50A	6.33U	144.50U	17596-2757	Envl 1.5
108	$18^h00^m05^s$	−20°51′07″	5.6	11.2	2.2	−10	L262	a
	8.9747	.6829	7.28A	4.15A	24.61U	203.80U	18001-2053	Core .7
			7.28U	5.08U	46.20U	265.90A	17598-2053	Envl 2.0
			5.18U	2.54A	52.98U	116.70U	17599-2034	Envl
109	$18^h01^m54^s$	−28°26′09″	9.6	3.4	3.4	0	SCHO741	a, C
	2.5870	−3.4313	.79A	1.74U	3.20U	119.00U	18018-2825	Core .3
			.66A	2.69U	4.35U	50.40U	18018-2820	Envl .8
110	$18^h03^m00^s$	−18°25′33″	6.1	5.6	1.1	−60	L307	b, E
	11.4207	1.2906	1.27A	1.03U	5.12U	87.65U	18032-1826	Core .5

TABLE 1—*Continued*

No. (1)	α_{1950} (2)	δ_{1950} (3)	V_{LSR} (4)	a (5)	b (6)	P.A. (7)	Other Names (8)	Comments (9)
	ℓ (10)	b (11)	$S_{12\mu m}$ (12)	$S_{25\mu m}$ (13)	$S_{60\mu m}$ (14)	$S_{100\mu m}$ (15)	PSC No. (16)	Location (17)
111	$18^h04^m18^s$	−18°21′40″	6.9	4.5	1.1	25	L310	a, C, E
	11.6323	1.0478						
112	$18^h06^m00^s$	−01°50′33″	13.7	3.4	2.2	45	L502(?)	b, E
	26.3582	8.6683						
113	$18^h07^m23^s$	−22°45′02″	10.4	12.3	7.8	−30	L249	b, C
	8.1548	−1.7256	1.02A	2.04U	24.10U	336.40U	18072-2241	Core 2.1
			1.09A	.68B	8.81U	85.98U	18075-2250	Core
			1.20A	1.42A	15.96U	157.80U	18077-2248	Core
			1.04A	2.23U	19.37U	232.50U	18067-2236	Envl 6.3
			1.86U	1.73A	3.77U	40.71U	18067-2245	Envl
			2.77A	1.63A	21.54U	194.60U	18075-2232	Envl
			3.84A	1.83A	20.53U	171.70U	18076-2239	Envl
			2.38U	6.54U	8.72A	259.00U	18078-2256	Envl
			.77A	2.28U	14.50U	247.40U	18078-2244	Envl
			11.11A	20.44A	6.23A	327.00U	18080-2238	Envl
			2.38A	6.54U	18.59U	351.60U	18081-2256	Envl
			9.25A	7.62A	19.42U	369.00U	18082-2251	Envl
114	$18^h09^m12^s$	−22°41′07″	11.9	3.4	2.2	0		b, E
	8.4155	−2.0605	6.57A	4.20A	16.79U	168.00U	18093-2241	Core .2
			1.58A	1.10A	16.32U	164.90U	18092-2244	Envl .5
115	$18^h09^m17^s$	−07°54′47″	3.9	2.2	2.2	0	L426	a
	21.3693	5.0630						
116	$18^h09^m19^s$	−22°46′09″	11.4	3.4	2.2	−80		b, E
	8.3555	−2.1257	1.58A	1.10A	16.32U	164.90U	18092-2244	Core .3
			1.83A	1.34B	14.28U	27.96B	18095-2246	Core
			9.18A	5.80A	14.90U	213.30U	18095-2243	Envl .8
117	$18^h09^m26^s$	−07°33′30″	1.7	2.2	2.2	0	L430	b
	21.7003	5.1995						
118	$18^h09^m43^s$	−15°50′00″	13.1	2.2	2.2	90		b
	14.4697	1.1524	1.32B	1.12A	4.82U	55.14U	18094-1550	Envl .8
119	$18^h11^m11^s$	−07°05′31″	5.3	2.2	1.1	40	L438	b, E
	22.3131	5.0531						
120	$18^h11^m23^s$	−07°09′26″	5.4	3.4	3.4	0	L438	b, E
	22.2867	4.9647	.34A	.26U	.79U	8.71U	18116-0707	Envl .3
121	$18^h11^m28^s$	−06°59′22″	5.7	2.2	2.2	0		b, E, I
	22.4438	5.0282	.25U	.34U	1.06U	8.07A	18115-0701	Envl .0
			4.34A	1.20A	.40U	4.44U	18116-0657	Envl
122	$18^h11^m46^s$	−07°08′52″	6.1	3.4	1.1	50	L438	b, E, C
	22.3395	4.8871	.34A	.26U	.79U	8.71U	18116-0707	Envl .0
			1.63A	1.21A	.79U	5.95U	18120-0709	Envl
123	$18^h11^m55^s$	−07°24′00″	8.6	4.5	2.2	−45	L436	b, E, C
	22.1351	4.7344						
124	$18^h12^m18^s$	07°03′39″	20.4	3.4	2.2	90	LBN102	a, H
	35.1228	11.3650	.25U	.25U	.41U	9.36A	18122+0703	Core .0

TABLE 1—*Continued*

No. (1)	α_{1950} (2)	δ_{1950} (3)	V_{LSR} (4)	a (5)	b (6)	P.A. (7)	Other Names (8)	Comments (9)
	ℓ (10)	b (11)	$S_{12\mu m}$ (12)	$S_{25\mu m}$ (13)	$S_{60\mu m}$ (14)	$S_{100\mu m}$ (15)	PSC No. (16)	Location (17)
			.25U	.55U	.53B	5.95A	18120+0704	Envl .0
125	$18^h12^m39^s$	−18°12′14″	6.4	12.3	7.8	0	B92,L323	b
	12.7322	−.6065	1.95U	4.15A	24.38U	377.80U	18126-1820	Core 1.8
			2.70A	1.86B	30.39U	226.80U	18127-1803	Core
			5.45A	6.08A	25.44U	610.90U	18121-1813	Envl 5.5
			15.11A	12.87A	31.38U	623.90U	18121-1825	Envl
			3.90B	12.08A	57.89U	623.80U	18122-1818	Envl
			4.18U	5.52U	75.32A	302.10U	18123-1829	Envl
			1.17B	1.35B	7.03A	548.50U	18126-1754	Envl
			1.17A	1.34U	22.29U	207.10U	18126-1758	Envl
			1.14A	4.15U	15.49U	197.50U	18128-1821	Envl
			1.39U	2.29A	26.54U	235.50U	18128-1824	Envl
			2.65A	2.07A	17.23U	193.50U	18129-1801	Envl
			2.55U	3.30U	13.66U	106.00A	18130-1824	Envl
			2.15A	1.94A	8.12B	419.70U	18132-1821	Envl
			2.49A	1.30A	27.31U	389.60U	18132-1804	Envl
126	$18^h12^m39^s$	−03°46′38″	9.2	3.4	2.2	−85	L490(?)	b, E
	25.4273	6.2894						
127	$18^h12^m40^s$	−16°27′12″	10.8	2.2	1.1	0		b
	14.2695	.2310	3.76A	12.12A	42.88U	213.30U	18126-1629	Envl .3
128	$18^h13^m11^s$	−03°52′14″	8.5	2.2	2.2	0	L492	b
	25.4065	6.1303	.25U	.26U	.58U	4.40A	18130-0352	Core .0
			2.39A	1.31A	.40U	16.66U	18132-0350	Core
129	$18^h13^m11^s$	−03°45′31″	6.5	5.6	3.4	−20	L492	b
	25.5057	6.1831	.42U	.32U	.55A	16.17U	18130-0341	Core .1
			.25U	.26U	.58U	4.40A	18130-0352	Envl .3
			2.39A	1.31A	.40U	16.66U	18132-0350	Envl
130	$18^h13^m38^s$	−02°33′52″	10.0	5.6	2.2	90	L507(?)	b
	26.6192	6.6456						
131	$18^h14^m04^s$	−18°03′52″	6.6	4.5	2.2	−50	B93,L328	b
	13.0166	−.8360						
132	$18^h17^m06^s$	−06°07′12″	6.6	6.7	5.6	−20	L466	b, E
	23.8780	4.2071	1.47A	.85A	.95U	7.16U	18173-0609	Core .3
			1.98A	.83A	.87U	6.18U	18167-0602	Envl 1.0
			.57A	.32U	.90U	8.52U	18167-0607	Envl
			6.80A	6.20A	1.54A	7.20U	18174-0612	Envl
133	$18^h19^m54^s$	−01°29′05″	4.7	2.2	1.1	−10		b
	28.3163	5.7634						
134	$18^h20^m09^s$	−01°44′14″	5.6	2.2	1.1	50		b
	28.2848	5.6627						
135	$18^h20^m33^s$	−20°47′14″	13.2	7.8	5.6	−80	L306	a
	11.3439	−3.4716	.28U	.35U	2.21B	27.29A	18203-2047	Core 1.3
			1.04A	.52U	.95U	12.41U	18204-2044	Core
			1.35A	1.02A	.92U	10.46U	18205-2049	Core
			7.47A	1.87A	.81U	12.02U	18203-2040	Envl 3.8

TABLE 1—*Continued*

No. (1)	α_{1950} (2)	δ_{1950} (3)	V_{LSR} (4)	a (5)	b (6)	P.A. (7)	Other Names (8)	Comments (9)
	ℓ (10)	b (11)	$S_{12\mu m}$ (12)	$S_{25\mu m}$ (13)	$S_{60\mu m}$ (14)	$S_{100\mu m}$ (15)	PSC No. (16)	Location (17)
			.50A	.49U	2.00U	28.17U	18205-2038	Envl
			.59U	.41U	1.66A	11.22U	18206-2041	Envl
			2.26A	1.31A	1.21U	9.15U	18211-2050	Envl
136	$18^h21^m11^s$	−01°19′09″	3.7	6.7	1.1	60	L533	b, E
	28.6127	5.5580						
137	$18^h21^m44^s$	−01°00′33″	9.1	13.4	4.5	65	L539	b, E
	28.9529	5.5798	.83A	.39A	.46U	4.45U	18219-0100	Core .5
			1.29A	.88A	.49U	6.38U	18223-0058	Envl 1.5
138	$18^h22^m11^s$	−10°54′43″	6.2	6.7	5.6	−80	L414	b
	20.2423	.8383	3.65U	2.93A	12.50A	219.70U	18221-1055	Core 1.0
			2.05A	3.85A	4.54U	49.74U	18216-1048	Envl 3.0
			2.04A	1.09B	20.01U	379.20U	18223-1101	Envl
139	$18^h22^m44^s$	−10°41′40″	5.8	4.5	3.4	30	B94,L416,L417	b, E
	20.4980	.8211	1.29A	.76A	22.52U	367.60U	18225-1043	Core .6
			.77A	2.27U	23.77U	291.50U	18225-1045	Envl 1.8
			4.66A	1.91A	21.26U	324.40U	18228-1037	Envl
140	$18^h23^m29^s$	−10°20′00″	5.9	6.7	2.2	−65	B96,L420(?)	b, E
	20.9044	.8270	3.86A	5.47A	26.34U	207.00U	18230-1019	Envl 1.3
			1.21A	3.97U	29.89U	215.60U	18239-1023	Envl
141	$18^h25^m04^s$	−11°29′26″	5.9	5.6	1.1	40	L411	b
	20.0647	−.0586	3.18U	3.23U	14.91A	200.00U	18252-1124	Envl 1.3
			3.30A	4.64U	437.00U	761.00U	18252-1129	Envl
142	$18^h27^m04^s$	−13°43′19″	18.6	3.4	2.2	0		a, E
	18.3217	−1.5350	.95A	.68A	10.18U	222.50U	18272-1343	Core .3
143	$18^h27^m34^s$	−17°45′00″	6.8	9.0	2.2	50	B311,L356	b
	14.8106	−3.5190	3.09A	.93A	10.68U	100.70U	18274-1743	Core .7
			1.71A	1.10A	.94U	73.89U	18274-1751	Envl 2.0
			4.96A	3.44A	6.67U	88.85U	18282-1739	Envl
144	$18^h27^m48^s$	−16°07′28″	15.9	2.2	1.1	60	L374(?)	a
	16.2773	−2.8120	1.15A	1.48A	10.02U	98.54U	18278-1608	Envl .3
145	$18^h29^m40^s$	−09°12′45″	4.5	9.0	3.4	−20	B100,L443	b, E
	22.6080	.0057	1.58A	4.03U	65.10U	267.00U	18296-0911	Core 1.3
			2.31U	4.18U	65.10A	150.60U	18293-0912	Envl 3.8
			4.50U	4.48U	37.85A	371.90U	18293-0906	Envl
			1.80A	4.52U	16.78U	285.60U	18294-0901	Envl
			3.01A	4.38A	16.84U	274.40U	18295-0920	Envl
			3.92U	2.17A	26.36U	228.30U	18300-0918	Envl
			2.21U	2.09A	36.69U	132.00U	18301-0914	Envl
146	$18^h29^m48^s$	−09°00′00″	4.3	6.7	4.5	35	B101	b, E
	22.8099	.0788	4.50U	4.48U	37.85A	371.90U	18293-0906	Envl 3.5
			1.80A	4.52U	16.78U	285.60U	18294-0901	Envl
			3.30U	3.96A	116.20A	485.50B	18295-0854	Envl
			9.22A	10.88A	103.60U	167.40U	18298-0904	Envl
			4.95U	4.98A	103.60A	490.50U	18299-0907	Envl
			4.71A	3.46U	174.10U	195.50U	18300-0856	Envl

TABLE 1—*Continued*

No. (1)	α_{1950} (2)	δ_{1950} (3)	V_{LSR} (4)	a (5)	b (6)	P.A. (7)	Other Names (8)	Comments (9)
	ℓ (10)	b (11)	$S_{12\mu m}$ (12)	$S_{25\mu m}$ (13)	$S_{60\mu m}$ (14)	$S_{100\mu m}$ (15)	PSC No. (16)	Location (17)
			2.97A	3.36A	24.84U	190.00U	18301-0900	Envl
			3.10A	19.87A	174.10A	435.10U	18301-0853	Envl
			7.92A	8.57A	41.05U	266.20U	18301-0902	Envl
147	$18^h30^m08^s$	−09°16′07″	4.5	5.6	4.5	70	B100,L443	b, E
	22.6106	−.1194	3.92U	2.17A	26.36U	228.30U	18300-0918	Core .8
			2.21U	2.09A	36.69U	132.00U	18301-0914	Core
			2.05B	2.07A	23.10U	674.10U	18302-0923	Envl 2.5
			6.49A	4.96B	31.77U	208.90U	18303-0910	Envl
148	$18^h30^m12^s$	−26°03′52″	6.5	3.4	2.2	−50	B98,L239	a
	7.6606	−7.8678	.25U	.43U	.41U	5.38A	18302-2603	Core .2
149	$18^h35^m19^s$	−13°46′38″	−2.0	6.7	2.2	50	B102,L401	a
	19.2027	−3.3355	.70A	.34U	6.18U	84.66U	18351-1348	Core .1
			.52A	.46U	7.49U	103.60U	18354-1350	Envl .3
150	$18^h36^m37^s$	13°20′40″	4.6	2.2	2.2	0		b
	43.5376	8.7933						
151	$18^h37^m02^s$	13°06′07″	4.8	7.8	2.2	0		b
	43.3634	8.5939						
152	$18^h39^m00^s$	−02°12′12″	4.4	3.4	3.4	0	B316,L555	b, E
	29.8928	1.2036						
153	$18^h39^m31^s$	−20°02′12″	6.2	4.5	2.2	20	B315,L346	a, C
	14.0629	−7.0766						
154	$18^h40^m05^s$	15°57′07″	5.9	5.6	4.5	0		b
	46.2816	9.1883						
155	$18^h44^m40^s$	−04°36′26″	6.4	11.2	3.4	−10	B104	b
	28.4124	−1.1620	1.94A	1.29A	23.35U	59.34B	18445-0440	Core 1.1
			4.58A	2.84A	10.74U	136.40U	18446-0435	Core
			.84A	2.34U	12.04U	122.90U	18447-0437	Core
			13.07A	3.48A	13.12U	201.30U	18445-0448	Envl 3.3
			.82U	.46U	3.51A	43.69U	18448-0426	Envl
156	$18^h46^m17^s$	−05°08′19″	3.6	4.5	3.4	−5	B106	b
	28.1249	−1.7622	2.04A	1.00A	14.65U	218.90U	18459-0506	Envl 1.0
			3.80A	2.57A	12.25U	86.94U	18460-0509	Envl
			1.02A	.52A	15.99U	194.60U	18464-0511	Envl
			1.14A	.60A	15.82U	202.20U	18464-0502	Envl
			4.28A	3.15A	14.13U	197.80U	18465-0507	Envl
157	$18^h50^m21^s$	−07°02′45″	16.4	6.7	3.4	40	B114,L514	a
	26.8929	−3.5375	.53A	.30B	5.62U	64.06U	18504-0705	Core .1
			1.15A	.64A	5.90U	67.15U	18504-0700	Core
			.60A	.30B	5.89U	56.42U	18501-0659	Envl .3
158	$18^h50^m39^s$	−06°43′17″	15.8	5.6	1.1	0	B115,L518	a
	27.2159	−3.4546	.43A	.27U	4.70U	56.93U	18506-0637	Envl .0
159	$18^h50^m41^s$	−06°50′00″	16.2	3.4	2.2	35	SCHO943	b
	27.1205	−3.5141						

TABLE 1—*Continued*

No. (1)	α_{1950} (2)	δ_{1950} (3)	V_{LSR} (4)	a (5)	b (6)	P.A. (7)	Other Names (8)	Comments (9)
	ℓ (10)	b (11)	$S_{12\mu m}$ (12)	$S_{25\mu m}$ (13)	$S_{60\mu m}$ (14)	$S_{100\mu m}$ (15)	PSC No. (16)	Location (17)
160	$18^h50^m58^s$	−07°29′17″	12.9	2.2	1.1	−60	B117	b
	26.6108	−3.9832	.37U	.32U	.78U	7.93A	18509-0729	Core .1
			1.33A	.42A	.51U	33.10U	18511-0727	Envl .3
161	$18^h51^m14^s$	−07°30′17″	12.6	3.4	1.1	80	B118	b
	26.6364	−4.0330	.37U	.32U	.78U	7.93A	18509-0729	Envl .0
			1.33A	.42A	.51U	33.10U	18511-0727	Envl
			4.65A	3.52A	.71A	30.13U	18515-0731	Envl
162	$18^h51^m42^s$	−07°17′41″	16.0	3.4	2.2	40	SCHO950	b
	26.8236	−3.9477						
163	$18^h51^m56^s$	−04°37′08″	4.2	2.2	1.1	−45	B119	b
	29.2339	−2.7751	.56A	.36U	10.89U	125.50U	18517-0435	Envl .3
			.25U	.28U	2.06U	18.27A	18520-0439	Envl
164	$18^h52^m12^s$	−04°39′55″	4.3	2.2	1.1	−45	B120	b
	29.2224	−2.8545	.25U	.28U	2.06U	18.27A	18520-0439	Core .2
165	$18^h53^m06^s$	−04°30′25″	5.0	3.4	1.1	−35	B322	b
	29.4678	−2.9842						
166	$18^h54^m08^s$	−04°49′26″	15.9	6.7	3.4	−20	B122,L545	a
	29.3036	−3.3581	3.63A	4.34A	.79U	55.69U	18543-0443	Envl .8
			.44A	.49A	1.00U	59.88U	18545-0457	Envl
167	$18^h54^m53^s$	−04°48′19″	10.0	4.5	3.4	80	B123,L546	b
	29.4057	−3.5154						
168	$18^h56^m21^s$	−04°36′40″	9.7	9.0	5.6	10	B126,L556	b
	29.7460	−3.7513	.77A	.61A	.93U	43.38U	18562-0437	Core .8
169	$18^h56^m46^s$	−04°35′00″	9.5	4.5	2.2	−45	B126,L556	b, C
	29.8180	−3.8298						
170	$18^h58^m52^s$	−05°31′40″	10.2	6.7	5.6	50	B127,L544	b
	29.2146	−4.7261	13.95A	8.49A	1.79A	30.58U	18587-0534	Core .6
			.53U	.46U	1.16A	7.71B	18588-0530	Core
			.56A	.25U	.56U	32.40U	18590-0539	Envl 1.8
			.81U	.39U	1.07A	7.88U	18593-0535	Envl
171	$18^h59^m02^s$	−04°38′19″	16.7	11.2	4.5	45	B128	b
	30.0270	−4.3565						
172	$18^h59^m05^s$	−05°26′05″	10.1	3.4	1.1	35		b, C
	29.3234	−4.7334						
173	$18^h59^m06^s$	−05°37′12″	10.7	3.4	2.2	90	B130	a
	29.1595	−4.8209	.56A	.25U	.56U	32.40U	18590-0539	Envl .0
			.81U	.39U	1.07A	7.88U	18593-0535	Envl
174	$18^h59^m18^s$	−05°38′19″	10.6	3.4	2.2	−55	B130	a
	29.1641	−4.8709	.81U	.39U	1.07A	7.88U	18593-0535	Core .0
			.56A	.25U	.56U	32.40U	18590-0539	Envl .0
175	$18^h59^m26^s$	−05°22′14″	10.1	6.7	3.4	55	B129,L549	a
	29.4206	−4.7819	.53U	.28U	.78A	19.22U	18594-0519	Core .3
			1.61A	1.21A	.69U	28.60U	18598-0522	Envl .8

TABLE 1—*Continued*

No. (1)	α_{1950} (2)	δ_{1950} (3)	V_{LSR} (4)	a (5)	b (6)	P.A. (7)	Other Names (8)	Comments (9)
	ℓ (10)	b (11)	$S_{12\mu m}$ (12)	$S_{25\mu m}$ (13)	$S_{60\mu m}$ (14)	$S_{100\mu m}$ (15)	PSC No. (16)	Location (17)
176	$18^h59^m35^s$	−04°27′08″	16.7	3.4	2.2	40		b
	30.2574	−4.3957						
177	$19^h00^m00^s$	17°40′00″	16.3	5.6	4.5	50	L708(?)	a
	49.9722	5.6858	.25U	.25U	.40U	5.65A	18599+1739	Core .4
178	$19^h00^m01^s$	18°05′00″	15.3	6.7	4.5	−40	L710	a
	50.3476	5.8706	.96A	.33A	.40U	2.37U	18595+1812	Envl .5
			.23A	.27U	.45U	2.95U	19002+1755	Envl
			.94A	.28A	.40U	2.68U	19002+1808	Envl
179	$19^h01^m57^s$	−05°25′35″	11.8	3.4	2.2	20		a
	29.6564	−5.3635	.25U	.25U	.75B	7.42A	19018-0525	Core .1
180	$19^h03^m31^s$	−06°58′07″	11.8	12.3	5.6	−30	B133,L531	b
	28.4530	−6.4106	.65U	.50U	.85A	13.61U	19034-0658	Core .3
			.57A	.28U	2.00U	12.13U	19035-0657	Core
			.25U	.50A	.98A	9.84B	19037-0659	Core
			.26A	.32U	2.06U	5.15U	19031-0659	Envl .8
			.25U	.25U	.41U	4.35A	19038-0712	Envl
181	$19^h04^m13^s$	−06°19′24″	11.3	5.6	3.4	−25	B134,L543	b
	29.1108	−6.2729						
182	$19^h10^m00^s$	17°52′45″	14.9	4.5	4.5	0	L714	b, E
	51.2576	3.6679						
183	$19^h11^m06^s$	16°29′28″	6.6	2.2	1.1	20		a, E
	50.1496	2.7888						
184	$19^h11^m38^s$	16°22′12″	6.3	3.4	2.2	−30	L709	b
	50.1033	2.6167	.97A	.58A	.98U	8.93U	19116+1623	Core .0
185	$19^h13^m21^s$	−01°24′28″	8.8	2.2	1.1	50	B137	a
	34.5544	−6.0520						
186	$19^h13^m32^s$	−01°21′40″	9.3	3.4	1.1	0	B137	a, C
	34.6176	−6.0719						
187	$19^h15^m28^s$	−01°33′19″	9.0	11.2	2.2	−65	B139,L619	b
	34.6692	−6.5923	.34A	.25U	.41U	3.01U	19162-0135	Envl .8
188	$19^h17^m56^s$	11°30′33″	7.1	2.2	1.1	−30		a, E, C
	46.5311	−1.0166	.27U	1.06A	3.93A	18.48B	19179+1129	Core .0
			.45A	.36U	3.93U	72.58U	19180+1127	Envl .0
189	$19^h18^m10^s$	11°24′57″	7.6	12.3	3.4	−15	L676	b, E
	46.4755	−1.1100	.45A	.36U	3.93U	72.58U	19180+1127	Core .8
			.96A	.50A	5.53U	82.50U	19183+1123	Core
			2.95A	1.07A	5.45U	71.62U	19184+1118	Core
			.27U	1.06A	3.93A	18.48B	19179+1129	Envl 2.3
			1.09A	2.22A	3.51U	87.21U	19180+1116	Envl
			.41U	1.59A	2.55U	105.70U	19180+1114	Envl
			.67A	1.15U	5.37U	107.50U	19181+1139	Envl
			.38U	.43A	5.59U	106.70U	19181+1112	Envl
190	$19^h18^m41^s$	23°23′52″	11.0	5.6	2.2	60	L771	b
	57.1017	4.4442	.25U	.25U	1.03A	6.61A	19186+2325	Core .1

TABLE 1—*Continued*

No. (1)	α_{1950} (2)	δ_{1950} (3)	V_{LSR} (4)	a (5)	b (6)	P.A. (7)	Other Names (8)	Comments (9)
	ℓ (10)	b (11)	$S_{12\mu m}$ (12)	$S_{25\mu m}$ (13)	$S_{60\mu m}$ (14)	$S_{100\mu m}$ (15)	PSC No. (16)	Location (17)
191	$19^h19^m13^s$	01°11′40″	8.9	3.4	1.1	−20		a, E
	37.5580	−6.1495						
192	$19^h21^m00^s$	12°20′00″	6.9	4.5	3.4	−40	L686	a, E, C
	47.6119	−1.2842	.38U	1.21A	6.63U	145.60U	19208+1222	Core .2
			.28U	.26U	2.18U	26.41A	19207+1219	Envl .5
			1.02A	.33B	6.55U	145.00U	19208+1226	Envl
193	$19^h21^m30^s$	11°01′07″	7.5	3.4	2.2	−50	L675	a, E, C
	46.5142	−2.0190	2.06A	1.06A	5.08U	73.57U	19211+1104	Envl .5
			.87A	.48A	4.35U	49.09U	19217+1103	Envl
194	$19^h27^m38^s$	14°28′21″	3.8	7.8	4.5	−65		b
	50.2644	−1.6757	1.71A	1.13A	4.69U	60.26U	19273+1433	Envl 3.5
195	$19^h32^m27^s$	12°07′52″	9.6	2.2	2.2	45	L701	a
	48.7833	−3.8364						
196	$19^h32^m55^s$	12°13′07″	9.8	3.4	2.2	−30	B334	a
	48.9148	−3.8925	.25U	.27U	.40U	3.98A	19329+1213	Core .0
197	$19^h33^m53^s$	18°16′52″	24.5	3.4	3.4	0		b, E
	54.3222	−1.1299						
198	$19^h34^m15^s$	12°12′54″	9.8	3.4	2.2	75	B336,L702	b
	49.0719	−4.1805	1.24U	.25U	.44U	3.87A	19342+1213	Core .1
199	$19^h34^m33^s$	07°27′45″	8.4	5.6	4.5	45	B335,L663	b
	44.9332	−6.5501	.32A	.25U	.40U	2.77U	19343+0727	Core .0
			.25U	.25U	8.29A	41.96A	19345+0727	Core
			1.95A	.89A	.40U	41.96U	19347+0729	Core
			.42A	.25U	.40U	41.96U	19348+0724	Envl .0
200	$19^h39^m09^s$	11°06′55″	9.6	3.4	2.2	60	B143,L700	b
	48.6972	−5.7620						
201	$19^h39^m49^s$	11°14′57″	9.7	5.6	4.5	−15	SCHO1080	a
	48.8962	−5.8400	.25U	.40U	.40U	4.73A	19398+1116	Core .2
202	$19^h40^m18^s$	18°45′00″	18.1	2.2	2.2	90		a
	55.4826	−2.2178						
203	$19^h41^m43^s$	18°57′45″	15.8	5.6	2.2	−40	SCHO1091(?)	b, E
	55.8352	−2.4023	.75A	.47A	.43A	19.24U	19413+1902	Envl .5
204	$19^h42^m16^s$	08°30′31″	7.6	5.6	2.2	80	L680	b
	46.7909	−7.7127						
205	$19^h43^m25^s$	27°45′00″	15.8	10.1	6.7	45	L810	a, R
	63.6241	1.6878	1.07A	4.91A	30.13A	83.97B	19433+2743	Core 1.1
			4.15A	2.69A	.56U	52.77U	19427+2741	Envl 3.3
			.69A	.47A	.76U	59.63U	19433+2751	Envl
			.26U	.25U	2.54A	13.52A	19438+2757	Envl
			.85A	.37A	.72U	60.90U	19438+2737	Envl
			1.53A	.85A	.98U	42.55U	19439+2748	Envl
206	$19^h44^m11^s$	18°55′07″	15.2	6.7	3.4	50	L758	a
	56.0917	−2.9300						

TABLE 1—*Continued*

No. (1)	α_{1950} (2)	δ_{1950} (3)	V_{LSR} (4)	a (5)	b (6)	P.A. (7)	Other Names (8)	Comments (9)
	ℓ (10)	b (11)	$S_{12\mu m}$ (12)	$S_{25\mu m}$ (13)	$S_{60\mu m}$ (14)	$S_{100\mu m}$ (15)	PSC No. (16)	Location (17)
207	$19^h44^m20^s$	21°06′07″	7.6	6.7	2.2	−65		b
	57.9935	−1.8542	.40B	.38A	3.49U	38.50U	19437+2108	Envl 2.0
208	$19^h45^m00^s$	18°47′12″	15.3	2.2	2.2	0	SCHO1106	b, R
	56.0737	−3.1605	.25U	.25U	.99A	9.98A	19450+1847	Core .2
209	$19^h45^m14^s$	18°16′52″	16.1	6.7	1.1	−45	SCHO1105	a
	55.6664	−3.4662						
210	$19^h52^m46^s$	33°39′26″	9.7	3.4	3.4	0	L832	b
	69.7321	2.9852	.48A	.32U	.76U	50.18U	19529+3341	Core .1
211	$19^h57^m40^s$	24°47′13″	6.9	2.2	2.2	0	L802	a, E
	62.7396	−2.5802	.41U	.35U	.71A	11.95A	19576+2447	Core .0
212	$19^h57^m52^s$	18°58′52″	16.6	5.6	2.2	0		a
	57.8114	−5.6707						
213	$19^h59^m24^s$	24°34′24″	7.6	2.2	2.2	0	L805	a, E
	62.7664	−3.0261						
214	$20^h01^m55^s$	26°30′45″	9.9	6.7	2.2	0	L814(?)	b, E
	64.7104	−2.4695	.21A	.52A	.88A	21.58U	20018+2629	Core .1
215	$20^h02^m10^s$	26°37′28″	9.1	2.2	2.2	45	L814(?)	a, E
	64.8350	−2.4567						
216	$20^h03^m38^s$	23°17′45″	12.6	6.7	4.5	50	L797	b, E
	62.2021	−4.5272	1.87A	5.57A	10.95A	17.65B	20037+2317	Core .1
217	$20^h05^m54^s$	36°57′07″	...	4.5	2.2	90	L863	
	73.9515	2.4649						
218	$20^h10^m42^s$	−01°30′00″	9.8	7.8	2.2	10	LBN111	a, B
	41.3385	−18.7704						
219	$20^h17^m37^s$	63°43′12″	−1.8	2.2	1.1	45	LBN444	a, B
	97.8373	15.3305	.25U	.25U	.40U	2.64A	20176+6343	Core .0
220	$20^h23^m00^s$	67°52′09″	2.9	2.2	2.2	90		a
	101.8185	17.0335						
221	$20^h29^m34^s$	25°49′39″	13.8	3.4	2.2	75		a
	67.6335	−7.9938						
222	$20^h32^m44^s$	63°51′07″	0.1	3.4	2.2	0	L1094	a, B
	98.8929	14.0033	.25U	.25U	.53A	3.97A	20328+6351	Core .0
223	$20^h34^m00^s$	64°00′20″	−2.6	3.4	1.1	90		a, B
	99.1039	13.9777						
224	$20^h35^m29^s$	63°42′45″	−2.7	3.4	3.4	0	L1100(?)	a, B
	98.9547	13.6743	.26B	.90A	2.99A	8.19A	20355+6343	Core .0
225	$20^h36^m35^s$	56°07′45″	−2.5	7.8	3.4	−20		a
	92.7775	9.1049	.25U	.25U	.43U	6.24A	20365+5607	Core .1
226	$20^h47^m09^s$	59°27′12″	−1.9	5.6	2.2	70	B148	a
	96.3197	10.0126						

TABLE 1—*Continued*

No. (1)	α_{1950} (2)	δ_{1950} (3)	V_{LSR} (4)	a (5)	b (6)	P.A. (7)	Other Names (8)	Comments (9)
	ℓ (10)	b (11)	$S_{12\mu m}$ (12)	$S_{25\mu m}$ (13)	$S_{60\mu m}$ (14)	$S_{100\mu m}$ (15)	PSC No. (16)	Location (17)
227	$20^h48^m09^s$	59°20′00″	−2.0	4.5	2.2	90	B149	a
	96.3044	9.8384						
228	$20^h50^m00^s$	56°04′26″	−1.7	3.4	1.1	45		a
	93.8960	7.5985						
229	$20^h53^m00^s$	68°07′00″	3.4	3.4	2.2	−45	L1171	a, H
	103.6978	14.8691						
230	$21^h16^m56^s$	68°05′43″	2.9	3.4	2.2	0	L1177	b, R, H
	105.1798	13.1621	.25U	.68A	11.75A	33.53A	21169+6804	Core .0
231	$21^h32^m18^s$	54°28′06″	6.5	5.6	4.5	0	B157	b
	96.9111	2.1625						
232	$21^h35^m17^s$	43°08′03″	12.6	5.6	2.2	20	B158	b
	89.6609	−6.6199	1.02A	3.55A	6.86A	13.89B	21352+4307	Core .1
233	$21^h39^m00^s$	57°34′26″	−0.9	5.6	3.4	15	B161	b
	99.6578	3.8319						
234	$21^h39^m46^s$	70°04′52″	−5.0	7.8	6.7	0	LBN515	a, H
	108.0996	13.1539						
235	$21^h54^m42^s$	58°46′52″	−1.8	3.4	2.2	−40	L1142	a
	102.0289	3.4496	.28A	.25U	.48U	31.21U	21548+5843	Envl .3
236	$22^h03^m46^s$	59°18′55″	−3.0	2.2	1.1	50	L1166	a
	103.2840	3.1770						
237	$22^h05^m42^s$	59°25′33″	−3.2	4.5	1.1	90	B173, L1169(?)	a
	103.5482	3.1236						
238	$22^h11^m15^s$	40°46′38″	0.2	4.5	3.4	60		a
	93.4650	−12.6309						
239	$22^h15^m51^s$	86°29′08″	...	13.4	5.6	−30		
	120.6057	24.6212						
240	$22^h31^m55^s$	58°18′00″	−3.6	3.4	2.2	45	L1192	a, H
	105.7899	.3439	.58A	.76A	6.89A	22.47A	22317+5816	Core .1
241	$23^h09^m40^s$	65°46′48″	−7.6	4.5	2.2	5	L1239	b
	113.0402	5.1142	.25U	.25U	.48U	7.43A	23095+6547	Core .0
242	$23^h09^m50^s$	61°22′45″	−10.9	5.6	3.4	30	L1225	b
	111.4123	1.0247						
243	$23^h23^m00^s$	63°20′00″	−11.1	10.1	2.2	−75	L1246	b
	113.5248	2.3225	.26B	.74A	2.06A	7.98B	23228+6320	Core .1
244	$23^h23^m51^s$	74°01′07″	3.9	11.2	5.6	70	L1262,L1261	b
	117.1269	12.3949	.25U	.78A	9.60A	15.20A	23238+7401	Core .0
			.40U	.33U	.86U	2.45A	23249+7406	Envl .0
245	$23^h52^m51^s$	58°34′40″	−0.8	2.2	2.2	0	SCHO1448	b, C
	115.7243	−3.2287						
246	$23^h54^m12^s$	58°17′47″	−0.5	7.8	4.5	−20	L1253	b
	115.8381	−3.5413						

TABLE 1—*Continued*

No. (1)	α_{1950} (2)	δ_{1950} (3)	V_{LSR} (4)	a (5)	b (6)	P.A. (7)	Other Names (8)	Comments (9)
	ℓ (10)	b (11)	$S_{12\mu m}$ (12)	$S_{25\mu m}$ (13)	$S_{60\mu m}$ (14)	$S_{100\mu m}$ (15)	PSC No. (16)	Location (17)
247	$23^h54^m54^s$	64°32′45″	−3.7	4.5	2.2	0	L1263	b
	117.2269	2.5525	.32A	1.11A	1.63A	14.03U	23550+6430	Envl .3
248	$23^h59^m16^s$	47°49′26″	−9.5	4.5	1.1	70		b, B
	114.4359	−13.9495						

COMMENTS.—(a) This work; (b) MWO data, 1988 March.

at least a factor of 2–3), since the reference regions are dominated by 12 μm detections and the core regions by 100 μm detections.

b) CO *Observations*

Several of the clouds were surveyed for lines of CO and ^{13}CO by us and other authors. Our observations were performed in the $J=1$–0 (2.6 mm) lines of CO and ^{13}CO at the Five College Radio Astronomy Observatory during 1986 May and October, and in the $J=2$–1 (1.3 mm) line of ^{12}CO at the Millimeter Wave Observatory in 1987 April. Data for cloud maps were collected in position-switched mode using reference positions which were observed in frequency-switched mode to verify their cleanliness. These position-switched spectra typically had 10:1 signal-to-noise ratios with either 0.033 km s^{-1} resolution (FCRAO) or 0.082 km s^{-1} resolution (MWO). The mean line-center LSR velocities are listed in column (4) of Table 1.

At the MWO, many (97) of the cataloged cloud central positions were surveyed for lines of ^{12}CO. Table 2 summarizes the MWO observations. For these data, frequency switching was generally used with 250 kHz wide filters (0.33 km s^{-1}) typically covering LSR velocities of −40 to +40 km s^{-1}. Continuum scans across the planets established the main-beam efficiency $\eta_{MB}=0.66$. The observed line intensities T_A^* were corrected for this efficiency to yield values of T_R appropriate to clouds not greatly extended with respect to the beam size (measured to be 67″). However, because of changing weather conditions, the line intensities reported here have uncertainties of 10%–30%. The line-center velocities and line widths should be expected to have much smaller uncertainties due to weather. The dominant effect on these quantities was produced during the reduction of the large standing waves in the spectra obtained. However, the reductions introduced no more than 0.3–0.5 km s^{-1} shifts to the line-center velocities and less than 25% changes to the line widths. In a few instances, multiple lines were seen toward a cloud position, indicating that the line of sight was also passing through a foreground or background cloud. Where the actual velocity assignment could not be performed (by checking a reference position, for example), all line velocities were listed.

IV. DISCUSSION

a) *Optical Properties*

Figure 1 shows the histogram of apparent mean optical sizes ($\sqrt{ab}$) for the clouds. Previously cataloged clouds are indicated in black. The mean size is 4′, and the numbers of larger sized clouds are affected by our selection being biased toward the smaller clouds. The new, uncataloged clouds represent 31% of the clouds smaller than 4′ and 23% of the clouds larger than that. The completeness of the catalog is poorest along the most opaque portions of the Galactic plane, for smaller clouds (1′–2′) in regions of low stellar density, and for larger clouds because of the selection bias. Hence, Figure 1 does not reflect the true cloud size distribution.

Figure 2 shows the histogram of cataloged optical ellipticities for the clouds. The mean ellipticity of 2.0 is indicated on the figure. The largest ellipticity is about 7. There are very few clouds (9%) with ellipticities between 3 and the maximum of 7. The lack of an ellipticity selection criterion is apparent in the low value of the number of very round clouds versus the number of those with ellipticities up to about 3. Most of these clouds are not round. This finding has serious impact on the nature of the models of structure and radiative transfer normally calculated for clouds of this type (e.g., Lee and Rogers 1987). More attention to the nonspherical cases is necessary to model properly the optical structures seen.

b) *Galactic Distributions*

The distribution of the clouds in Galactic coordinates l and b is shown in Figure 3. There the previously cataloged clouds are indicated by open circles and the previously uncataloged clouds by filled circles. Although there are some small distributional differences (more cataloged clouds near $l=110°$, $b=0°$; more uncataloged clouds near $l=30°$, $b=0°$), the overall distributions of previously cataloged and uncataloged clouds are roughly similar.

Also plotted on the figure are the general boundaries for three well-studied regions of star formation. The boundaries for the Taurus region correspond to the region mapped by Ungerechts and Thaddeus (1987). The Orion region corre-

TABLE 2

MWO DATA SET

Number (1)	T_R (K) (2)	V_{LSR} (km s^{-1}) (3)	ΔV (km s^{-1}) (4)	σ (K) (5)	Filters (kHz) (6)	Mode (7)	Comments (8)
1.....	2.77	−3.22	3.84	0.52	250	FS	
2.....	3.97	−2.40	1.78	0.64	250	FS	
3.....	6.43	38.32	3.08	0.42	250	FS	
6.....	6.18	12.50	0.71	0.14	250	FS	
10.....	< 0.78	...	...	0.26	250	FS	
13.....	3.13	35.90	1.28	0.41	250	FS	Low quality
14.....	7.84	11.01	2.49	1.36	250	FS	
15.....	5.40	0.77	5.99	0.83	250	FS	
16.....	5.92	−2.17	1.56	1.41	250	FS	Poor quality
17.....	5.24	−4.65	0.99	0.75	62.5	PS	
18.....	4.67	−2.87	1.52	0.34	250	FS	
20.....	8.06	5.68	0.84	0.55	62.5	PS[a]	
21.....	2.57	6.78	1.20	0.35	250	FS	
22.....	3.05	2.50	2.58	0.69	250	FS	
24.....	4.69	4.60	0.88	0.97	62.5	PS	
25.....	4.29	5.20	0.70	0.24	62.5	PS[a]	
28.....	13.90	8.83	1.00	0.91	250	FS	
42.....	4.48	2.80	2.23	0.49	250	FS	
43.....	5.02	3.31	2.30	0.41	250	FS	
47.....	3.25	19.32	1.35	0.39	250	FS	
49.....	4.82	9.59	4.59	0.36	250	FS	Self-absorbed?
50.....	7.00	0.89	0.65	0.64	250	FS	
52.....	5.06	16.63	4.03	0.28	250	FS	
54.....	6.26	19.49	4.51	0.76	250	FS	
55.....	3.40	20.32	1.22	0.81	250	FS	
59.....	3.19	10.59	2.63	0.35	250	FS	
63.....	7.11	2.54	0.85	0.47	250	FS	
64.....	3.19	0.46	1.32	0.37	250	FS	
68.....	7.96	4.98	1.42	0.76	62.5	PS[a]	
72.....	14.22	4.74	1.15	0.77	250	FS	
73.....	10.22	13.77	1.59	0.44	250	FS	
74.....	11.47	3.84	2.04	0.67	250	FS	
75.....	3.03	9.47	2.91	0.51	250	FS	Low quality
77.....	6.20	−0.32	0.95	0.50	250	FS	
79.....	10.17	3.55	2.14	0.90	250	FS	
80.....	9.94	2.57	1.00	2.41	250	FS	
81.....	10.59	3.40	2.05	1.35	250	FS	
83.....	7.57	4.98	0.65	0.38	250	FS	
84.....	10.89	4.68	0.80	0.27	250	FS	
87.....	12.73	4.66	0.95	1.07	250	FS	
88.....	15.58	3.60	1.37	1.41	250	FS	
92.....	4.54	10.51	2.38	0.46	250	FS	Globule line
	3.07	5.18	2.68	0.46	250	FS	
100.....	5.99	4.64	1.37	0.53	250	FS	
106.....	5.38	6.22	2.06	0.51	250	FS	
108.....	18.21	5.60	1.87	0.80	250	FS	
109.....	2.30	9.61	1.01	0.32	250	FS	
112.....	< 2.22	...	...	0.74	250	FS	
115.....	1.58	3.85	1.02	0.47	250	FS	
124.....	3.00	20.39	4.21	0.22	250	FS	
135.....	6.65	13.20	2.74	0.49	250	FS	
142.....	9.10	18.63	1.74	0.42	250	FS	
144.....	12.95	15.94	1.50	0.69	250	FS	
148.....	6.96	6.49	0.63	0.65	62.5	PS[a]	
149.....	1.55	−2.00	1.88	0.25	250	FS	Low quality
153.....	2.86	6.15	1.11	0.50	250	FS	Low quality
155.....	3.95	10.43	1.74	0.83	250	FS	
157.....	4.63	16.36	1.62	0.27	250	FS	
158.....	4.38	15.80	1.66	0.76	250	FS	
161.....	< 2.13	...	...	0.71	250	FS	
166.....	2.00	15.88	2.10	0.31	250	FS	Low quality
167.....	<1.65	...	...	0.55	250	FS	Low quality
173.....	6.05	10.67	1.02	0.57	250	FS	
174.....	5.43	10.61	1.38	0.57	250	FS	
175.....	3.39	10.14	1.62	0.66	250	FS	

TABLE 2—*Continued*

Number (1)	T_R (K) (2)	V_{LSR} (km s^{-1}) (3)	ΔV (km s^{-1}) (4)	σ (K) (5)	Filters (kHz) (6)	Mode (7)	Comments (8)
177.....	5.61	16.28	1.64	0.42	250	FS	Globule line
	3.67	5.72	1.87	0.42	250	FS	
178.....	4.46	15.33	0.85	0.60	250	FS	Globule line
	4.46	5.56	1.40	0.60	250	FS	
179.....	4.82	11.83	1.30	0.76	250	FS	
183.....	3.18	6.61	0.53	0.86	62.5	PS	
185.....	3.16	8.83	0.93	0.53	250	FS	
186.....	2.08	9.26	1.21	0.25	250	FS	Globule line
	1.90	13.69	1.48	0.25	250	FS	
188.....	4.19	7.12	4.40	0.42	250	PS[a]	
191.....	3.09	8.93	0.75	0.47	250	FS	
192.....	4.66	6.85	2.53	0.37	250	FS	
193.....	3.92	7.51	2.31	0.41	250	FS	
195.....	5.07	9.62	0.63	0.88	62.5	PS	
196.....	3.88	9.77	0.97	0.27	250	FS	
201.....	3.30	9.71	0.92	0.35	250	FS	Globule line
	1.36	−0.34	1.91	0.35	250		
	1.90	22.54	2.60	0.35	250	FS	
202.....	3.82	18.12	0.76	0.70	62.5	PS[a]	
205.....	5.48	15.77	3.38	0.58	250	FS	Poor quality
209.....	4.10	16.07	1.10	0.39	250	FS	
211.....	1.97	6.93	3.14	0.31	250	FS	
	4.31	24.42	1.85	0.31	250	FS	
212.....	5.86	16.64	1.48	0.64	250	FS	
213.....	1.79	7.60	1.16	0.24	250	FS	
216.....	<1.26	...	...	0.42	250	FS	
218.....	5.21	9.84	0.97	0.51	250	FS	
219.....	4.42	−1.83	0.51	0.47	62.5	FS	
220.....	5.66	2.87	1.26	1.12	250	FS	
221.....	3.15	13.81	1.89	0.55	250	FS	
222.....	1.95	0.05	1.37	0.30	250	FS	
223.....	3.24	−2.63	0.79	0.39	250	FS	
224.....	3.38	−2.73	2.73	0.48	250	FS	
225.....	4.10	−2.46	2.87	0.37	250	FS	
228.....	2.99	−1.65	0.79	0.69	62.5	PS	
229.....	3.82	3.40	0.78	0.47	250	FS	
234.....	4.35	−4.96	1.75	0.41	250	FS	
238.....	6.33	0.23	1.60	0.41	250	FS	
240.....	4.72	−3.61	0.87	0.65	250	FS	

[a] Map.

sponds to the region mapped by Maddalena *et al.* (1986). The Ophiuchus region was chosen to include the ρ Oph cloud in the southern end of the region and the L204 cloud complex of upper Scorpius in the northern region. Notice that although there are some clouds in these special regions, the vast majority of the clouds in Table 1 reside outside these star formation regions. In an effort to avoid *environmental* effects dominating the bulk characteristics of the sample, an attempt was made to obtain clouds from all over the sky and not to concentrate attention on the few well-studied regions indicated in the figure. Thus cloud characteristics for the whole sample are not influenced by special formation events which may have created or altered the Taurus dark clouds, for example.

The individual Galactic longitude and latitude distributions are shown in Figures 4 and 5, where the latitude distribution (Fig. 4) has been folded about $b = 0°$. If the raw counts in Figure 4 are normalized by the solid angle subtended by each bin, the dashed distribution is found. This distribution reflects two effects. First, we expect that most of these clouds are nearby (distance ≤ 1 kpc) because of the small number of foreground stars toward the cloud cores. The width of the distribution in b then reflects the proximity of the sample. If the scale height is similar to that seen for larger molecular clouds ($\Delta Z_{FWHM} \sim 120$ pc; Clemens, Sanders, and Scoville 1988), then the 10°–12° width implies a mean distance of $\sim$ 600 pc. Second, the lack of a central peak in the normalized (*dashed*) distribution in Figure 3 is probably a result of a bias against selecting clouds near the Galactic equator, where confusion and overlap of cloud boundaries hamper finding well-isolated small clouds.

The strong peak at longitudes 0°–30° (Fig. 5) is likely caused both by the larger number of background stars there (especially in the red, since most of those clouds were measured on the POSS E plates) and by the presence of reasonably nearby large molecular cloud complexes (M16, M17, etc.).

Since most of the clouds are not round, it is reasonable to test whether the orientation angles of the clouds are correlated with the direction of the Galactic plane at the location of the clouds. Figure 6 shows the histogram of angular

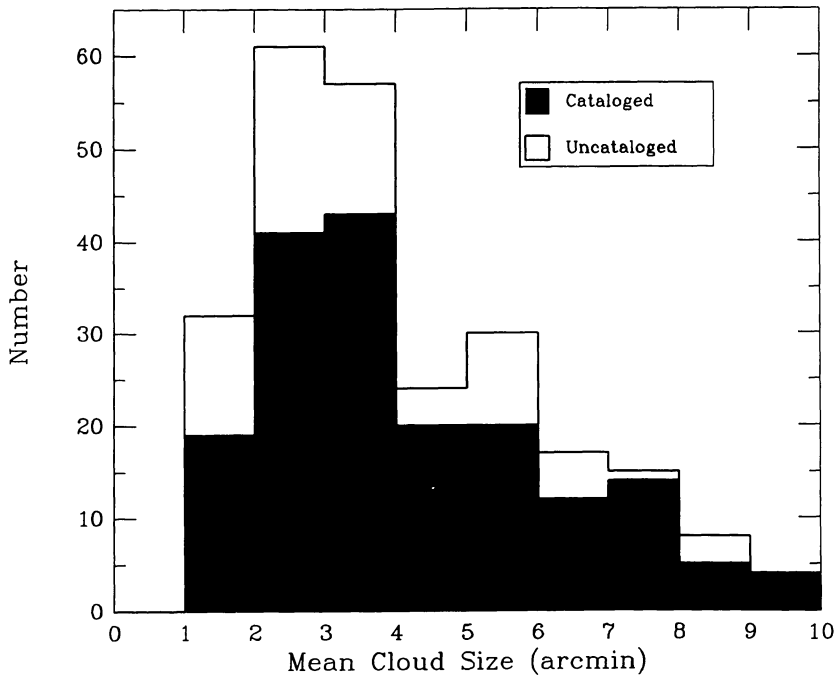

FIG. 1.—Distribution of mean sizes ($\sqrt{ab}$) for the cataloged optically opaque cores. "Cataloged" refers to a previous listing in other dark or bright cloud catalogs. "Uncataloged" refers to newly discovered globules.

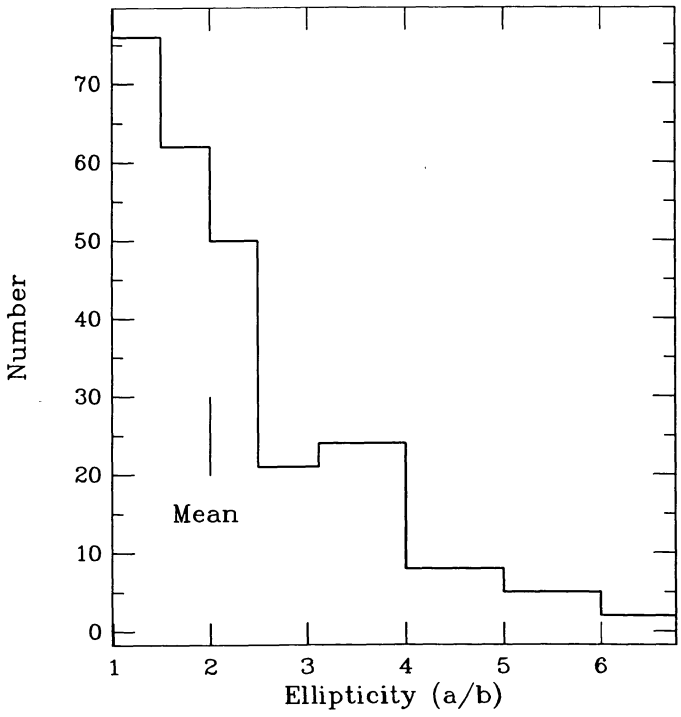

FIG. 2.—Ellipticity (a/b) distribution for the cataloged clouds. The mean ellipticity, 2.0, is indicated. The maximum ellipticity found was 7.0.

differences between the direction of the Galactic plane (the direction of increasing Galactic longitude) and the position angle of each cloud for the clouds with ellipticities greater than unity. There is no apparent trend of the cloud position angles with respect to the local Galactic plane. Whatever the formation and evolution mechanisms for the clouds are, the clouds retain no memory of the Galactic plane orientation in their optical shapes.

c) *Infrared Properties*

A total of 346 *IRAS* PSC sources were identified in 149 cloud cores and envelopes in the catalog of Table 1. Of these, 145 were found in the cores, with 51 predicted (from the reference region counts) to occur by chance, and 201 were found in the larger (3 times larger area) envelope regions, where 155 should have been seen by chance. Correcting for the chance hits and the ratio of areas, the core regions of the clouds registered PSC sources 6.1 times as frequently as the envelope regions. Clearly, *IRAS* did detect Bok globules.

The PSC tabulates the quality of the point-source template fit to the sources found along with their fluxes. Thus the relative pointlike or extended nature of sources can be determined from these correlation coefficients. Correlation coefficients of 100 have spatial profiles that are exact duplicates of the point-source response of the filters for that band. Coefficients below 95 indicate that the infrared source has some spatial structure which is more extended than a point source. For all of the 100 and 60 μm PSC detections in Table 1, the point-source correlation coefficients were collected and analyzed.

For core sources which were detected at 100 μm, the mean correlation coefficient was 98.18 for 74 sources, with an rms of

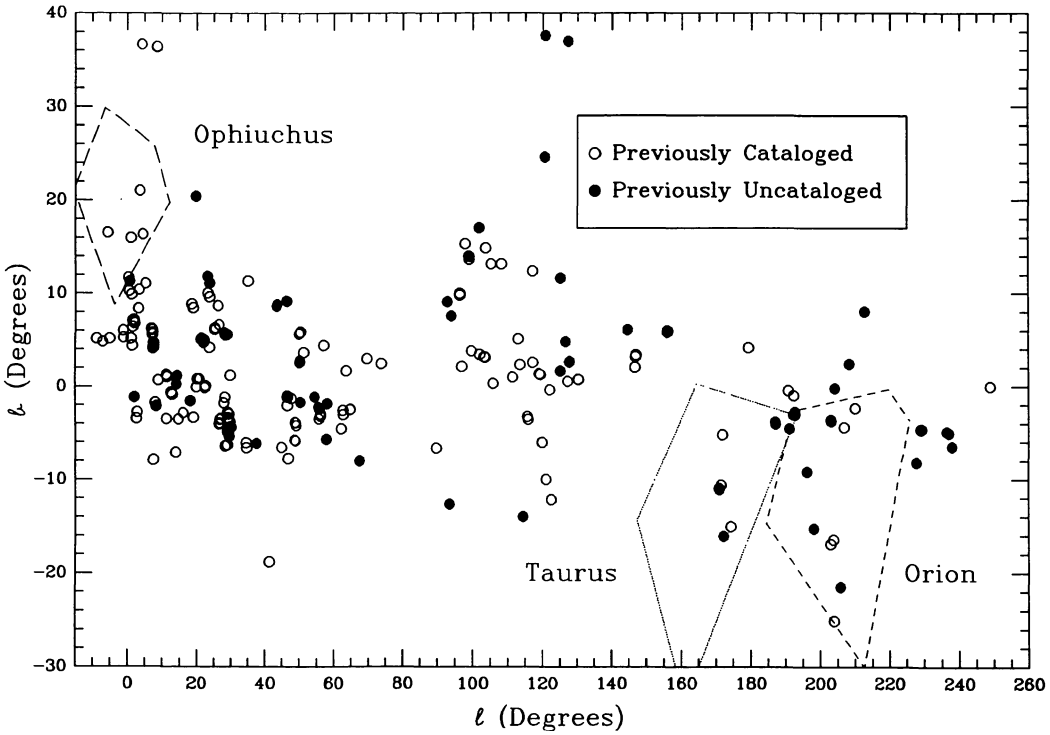

FIG. 3.—Galactic distribution of the clouds cataloged in Table 1. Previously cataloged clouds are shown as open circles, and previously uncataloged clouds as filled circles. Note that clouds often cluster and the symbols may cover several clouds. Also note that the latitude scale is 2.5 times the longitude scale. Three regions of star formation are indicated: Ophiuchus, Taurus, and Orion. Although there are some cataloged clouds in these regions, most of the clouds are outside these regions.

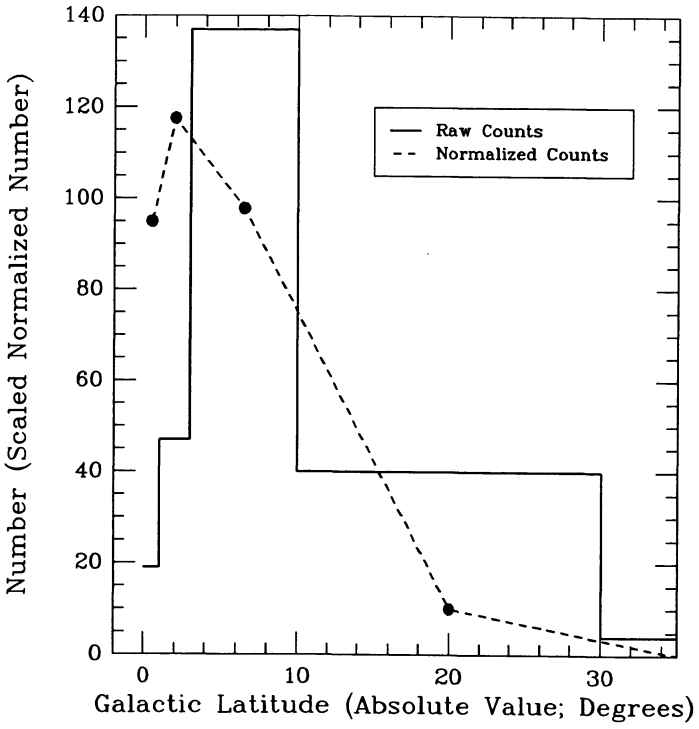

FIG. 4

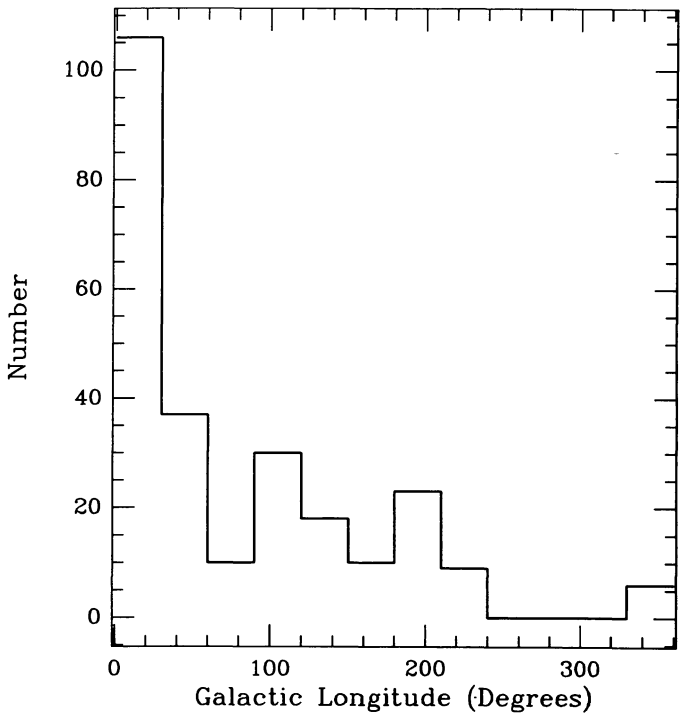

FIG. 5

FIG. 4.—Galactic latitude distributions of cataloged clouds. Raw counts and bin sizes are shown as a solid line; counts normalized by bin areas are shown as a dashed line. Note that the latitude axis has been folded about $b = 0°$.

FIG. 5.—Galactic longitude distribution of cataloged clouds

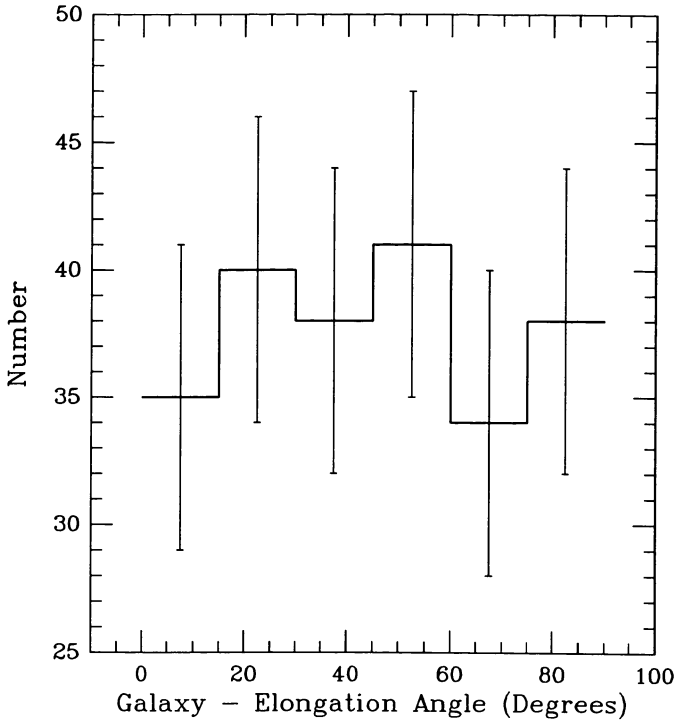

FIG. 6.—Distribution of difference angles between the Galactic plane and the ellongation axis of those clouds with nonunity ellipticities. That no trend is present is evidence against a strong influence of the Galactic plane on the physical structure, especially ellongation, of the clouds.

1.7. The actual distribution of coefficients for 100 μm had only two sources with coefficients below 95 (one at 94, one at 92). At 60 μm, for detected sources, the mean coefficient was also 98.18, for 56 sources, but with a somewhat larger rms of 2.2. Thus at 60 μm, six of the 56 sources had correlation coefficients below 95 (three at 94, three at 93).

Although one might argue that the eight sources with coefficients below 95 have flux values which are compromised, almost all of the PSC detections satisfy the criterion of being valid point sources. The presence of nearby cirrus and the extended nature of many of these clouds (Clemens 1988) do not seem to affect the PSC fluxes greatly.

The *types* of sources found in the three regions were also different, as shown in Figure 7. Each *IRAS* source in each region was characterized by the band showing the largest detected flux. The distributions were normalized by the total number of detections in each region and presented as normalized histograms in Figure 7. For the reference region (indicated by open triangles) the sources detected are dominated in number by those with bright 12 μm emission (i.e., stars). Similarly, the envelope distribution is indistinguishable from the reference region. However, the core sources are dominated by 100 μm detections. Once the core sources are corrected for each band (by the number of chance hits predicted by the reference region), the core distribution is almost entirely (90%) 60 and 100 μm dominated.

It is important to stress that the 100 μm core detections are *not* strongly affected by the presence of nearby 100 μm

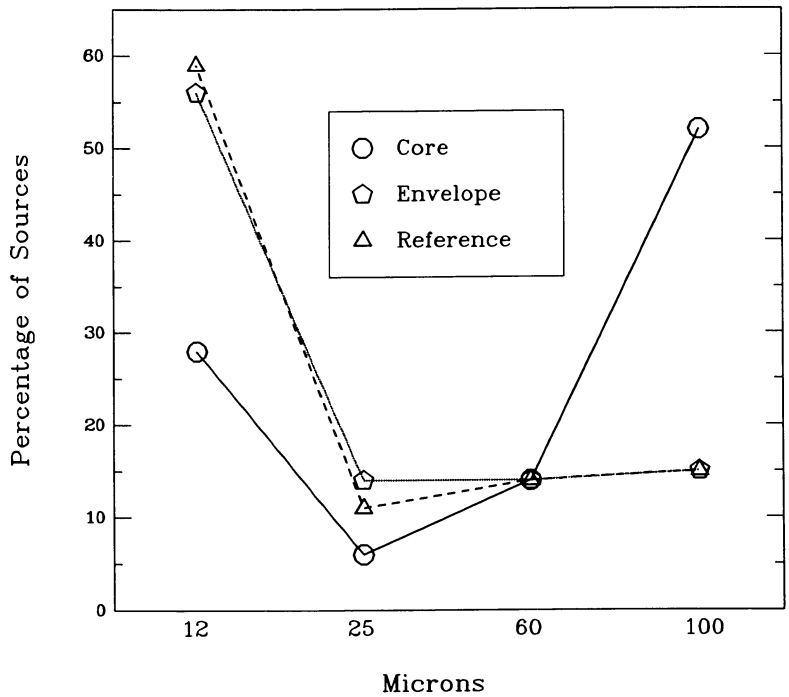

FIG. 7.—Normalized distributions of core, envelope, and reference *IRAS* PSC detections versus band containing dominant flux. Note that the reference and envelope regions are preferentially populated by sources with 12 μm dominant, while the core regions are populated by sources with 100 μm dominant.

infrared cirrus (Low *et al.* 1984). The PSC also contains a datum for each source which contains the number of 100 μm–only detections in a region $\frac{1}{2}° \times \frac{1}{2}°$ about the detected source. Although values greater than 3 for this CIRRUS1 flag are normally indicative of cirrus contamination (*IRAS Explanatory Supplement* 1985), contamination of this sample of *optically selected*, small molecular clouds requires values greater than about 36. The reasons are as follows. If our sample were *IRAS*–selected, then in a region $\frac{1}{2}° \times \frac{1}{2}°$ there would be three confusing sources along with a real source (for CIRRUS1 = 3), for a contamination level of 75%. However, for our optically selected sample, to contaminate the preselected positions the cirrus number density must be larger than for an *IRAS*–selected sample by the ratio of the areas of the CIRRUS1 region to the cloud area. For the mean cloud in our sample (4′ in diameter), a 50% chance of a random piece of cirrus appearing anywhere within the cloud boundary requires a CIRRUS1 density of 36.

The CIRRUS1 values for the PSC detections in the cloud cores were found to have a mean value of 6.6 with an rms of 2.4. We therefore estimate the *mean* contamination from cirrus to be about 9%, though a few of the larger clouds will exceed this somewhat. The better estimator of the contamination of *IRAS* sources for our clouds is contained in the reference regions chosen to surround the cataloged opaque cloud cores. There *are* contaminating sources found in the reference regions; however, they rarely are of the 100 μm–only variety. The cirrus contribution should appear equally in all three distributions of Figure 7. Yet, 100 μm–only sources are more strongly associated with the positions of the optically selected cloud cores than just outside those clouds. Hence the clouds exhibit bona fide cold *IRAS* detections (often below the 60 μm detector threshold; see § IV*c*[ii] below) with a vanishingly small amount of 100 μm cirrus contamination.

i) *Characteristics of the Core Sources*

Of the 145 core sources, 41 (with 31 predicted by chance) had $S_{12\ \mu m} \geq S_{25\ \mu m}$ or 12 μm–only detections and were thereby probably stars. For these 41 objects, the PSC lists three SAO stars (all K0 type), one Dearborn Observatory star, one galaxy, eight Lynds dark clouds (no stellar associations), and 28 entries with no associations.

The clues to the nature of these objects are likely contained in their Galactic distributions. The Galactic longitude distribution is strongly peaked between $l = 0°$ and $l = 30°$, and the latitude distribution is centered at $b = -0.°05$ with a width of less than 5°. Because the longitudes are almost all toward the Galactic nucleus and because the latitude distribution of these objects is even more confined to the Galactic equator than the whole sample (5° versus 12°), the objects giving rise to the 12 μm–dominated detections are likely background giant stars in the Galactic bulge. At FIR wavelengths bulge stars will suffer little extinction, and the sources found in the envelope and reference regions indicate that 30–40 12 μm–dominated sources should be found in the cores.

Because the number of these sources found in the cores is almost exactly that predicted from the envelope and reference regions, and because the distribution of these core objects closely follows the Galactic bulge distribution, we conclude that few, if any, of the clouds with 12 μm–dominated detections harbor embedded stars. These PSC detections all seem to be optically obscured, background stars.

The number of warm core sources with $S_{25\ \mu m} \geq S_{12\ \mu m}$ or 25 μm–only detections was eight. There were *no* sources in the sample which showed detected $S_{60\ \mu m} \geq S_{100\ \mu m}$, though 21 sources had detections at 60 μm and larger upper limits at 100 μm. The bulk of the sources (75) showed cool *IRAS* colors: $S_{100\ \mu m} \geq S_{60\ \mu m}$.

The core sources were split into two catagories, labeled bright and dark, to study their FIR properties further. Bright objects were those clouds with embedded reflection nebulae, bright rims, or cometary Hα extensions. Dark objects were the clouds with no associated bright nebulosity. The PSC detection rate was 40% (87 of 217) for the dark objects, but almost twice that, 71% (22 of 31), for the bright objects (some cores had multiple PSC detections). The optically bright objects also have a tendency to exhibit somewhat warmer $S_{60\ \mu m}/S_{100\ \mu m}$ colors and larger 100 μm fluxes than their darker counterparts, as shown below.

ii) *Comparison with Beichman et al. Cloud Cores*

It is useful to compare our PSC results with the results obtained by Beichman *et al.* (1986, hereafter BM) for embedded molecular cloud cores. The selection criteria used to associate *IRAS* sources with the BM cloud cores were somewhat different from our criteria, however. In addition to a positional requirement, they demanded detections in either the 25 μm band or in *both* the 60 μm and the 100 μm bands. These criteria were aimed at eliminating stars with only 12 μm emission, and infrared cirrus, with only 100 μm emission (although we have shown above that 100 μm–dominated sources associated with the smaller clouds do not suffer significant cirrus contamination). In the following discussion, we have applied the BM selection criteria to the PSC associations listed in our Table 1 to enable a uniform comparison.

Figure 8 shows the $\log(S_{12\ \mu m}/S_{25\ \mu m})$ versus $\log(S_{25\ \mu m}/S_{60\ \mu m})$ color-color diagram of the BM objects and the clouds in Table 1 with associated *IRAS* PSC sources having detections at 12, 25 and 60 μm. First, note that the two samples seem to be similarly distributed. Second, note that our clouds with detectable PSC emission in these bands tend either to populate the T Tauri zone or to show bright nebulosity. These PSC sources are likely embedded or erupted PMS stars, indicating that their associated small molecular clouds are active star-forming regions. Figure 9 shows the $\log(S_{25\ \mu m}/S_{60\ \mu m})$ versus $\log(S_{60\ \mu m}/S_{100\ \mu m})$ color-color diagram for the objects in our catalog and in the BM sample with detectable emission in those three bands. Again, the distributions are similar, although the BM sample seems to populate preferentially the warmer portion of the $S_{25\ \mu m}/S_{60\ \mu m}$ axis, while our sample is somewhat cooler.

Finally, Figure 10 shows the $\log(S_{60\ \mu m}/S_{100\ \mu m})$ versus $\log(S_{100\ \mu m})$ color-magnitude diagram for the two samples. There are several important points to note regarding this plot. First, the band of triangles in the lower left delineates the PSC 60 μm detection limit zone (the BM 60 and 100 μm detection criteria have been relaxed for those points in this plot). Second, the color difference between our sample and

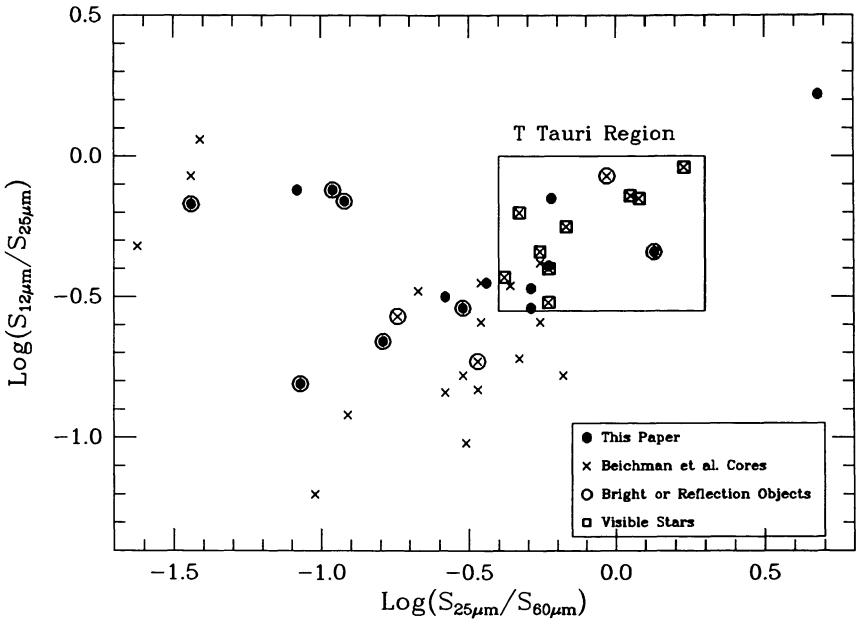

FIG. 8.—Comparison of the $S_{12\ \mu m}/S_{25\ \mu m}$ versus $S_{25\ \mu m}/S_{60\ \mu m}$ colors of our clouds with warm *IRAS* sources with those of the BM sample

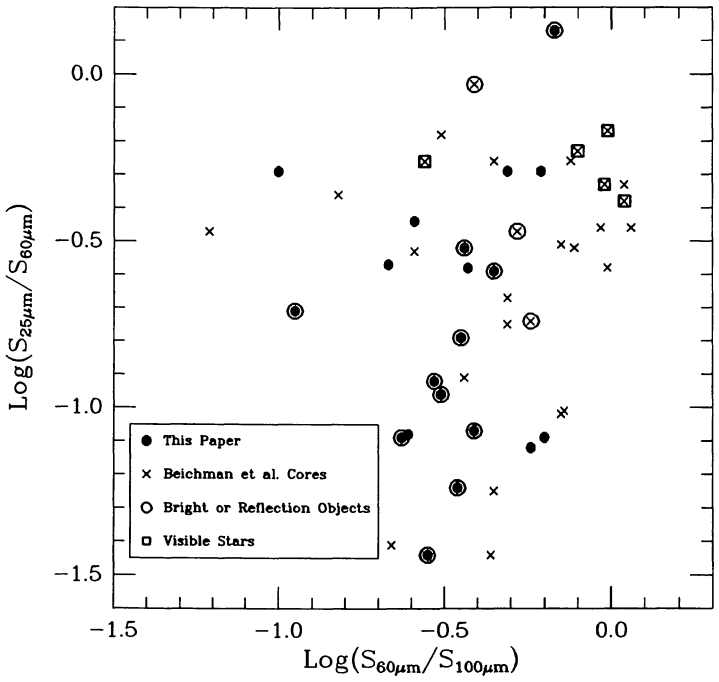

FIG. 9.—Comparison of the $S_{25\ \mu m}/S_{60\ \mu m}$ versus $S_{60\ \mu m}/S_{100\ \mu m}$ colors of our clouds with those of the BM sample

the BM sample found in the $S_{25\ \mu m}/S_{60\ \mu m}$ versus $S_{60\ \mu m}/S_{100\ \mu m}$ color-color figure is similarly represented here. When the log $(S_{60\ \mu m}/S_{100\ \mu m})$ colors are averaged, the mean of the BM sample is -0.35 ± 0.06 (~ 28 K for a λ^{-1} emissivity law) versus -0.66 ± 0.05 (~ 19 K) for our clouds (when the BM 60 and 100 μm criteria were used). When the $S_{60\ \mu m}/S_{100\ \mu m}$ colors are converted to temperatures (assuming a λ^{-1} emissivity) and averaged, the results are only mildly changed: 29 ± 2 K for the BM sample and 20 ± 1 K for ours. The mean 100 μm flux of the BM sample is also larger: 80 ± 30 Jy, versus 25 ± 5 Jy for our sample. Thus the BM sample of embedded molecular cloud cores seems warmer and more FIR-bright than our sample of isolated small clouds. The final point regarding this figure is that the four brightest 100 μm sources in the CB sample are all bright optical objects with nearly identical $S_{60\ \mu m}/S_{100\ \mu m}$ colors (-0.49 ± 0.03). These four clouds have either bright, stellar reflection nebulae (e.g., CB 205 = L810) or bright rims (e.g., CB 3 = LBN 594).

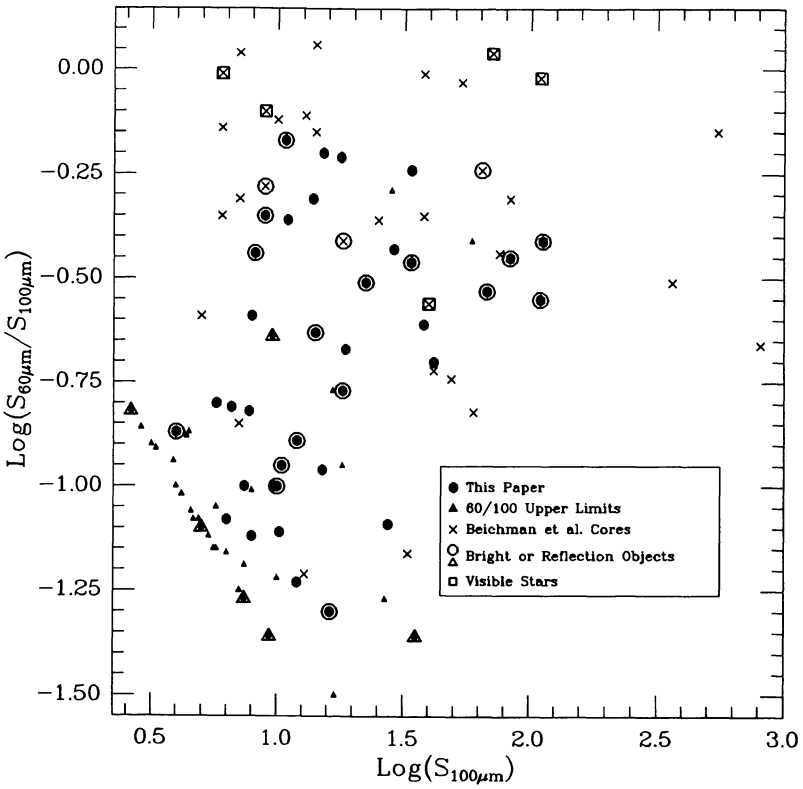

FIG. 10.—*IRAS* $S_{60\ \mu m}/S_{100\ \mu m}$ versus $S_{100\ \mu m}$ color-magnitude distribution of our clouds and BM clouds. The band of triangles at lower left delineates the zone of 60 μm upper limits.

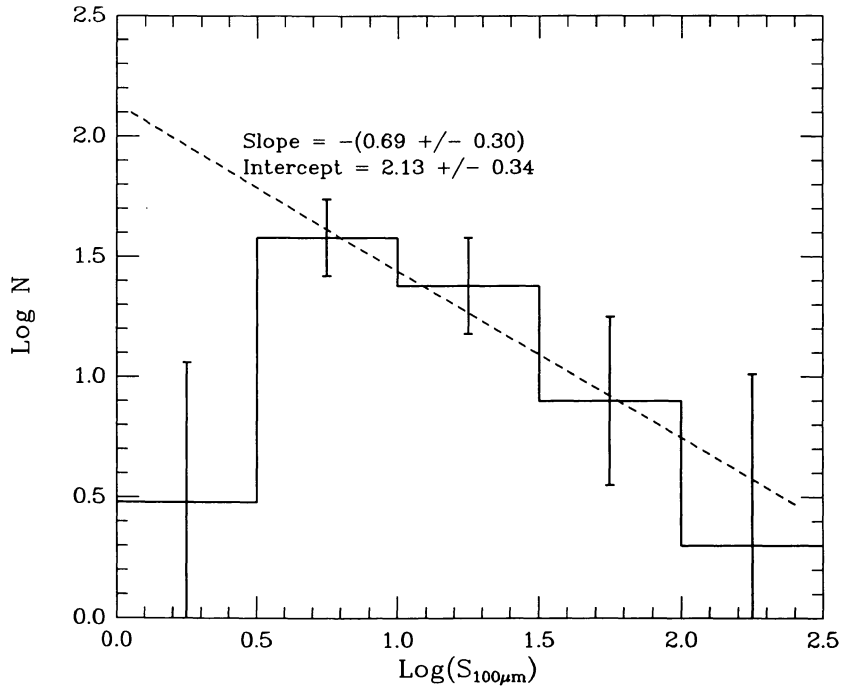

FIG. 11.—*IRAS* 100 μm flux distribution for our clouds. The dashed line represents the fit to the upper four flux bins. The lower flux bin is strongly affected by the PSC survey limits.

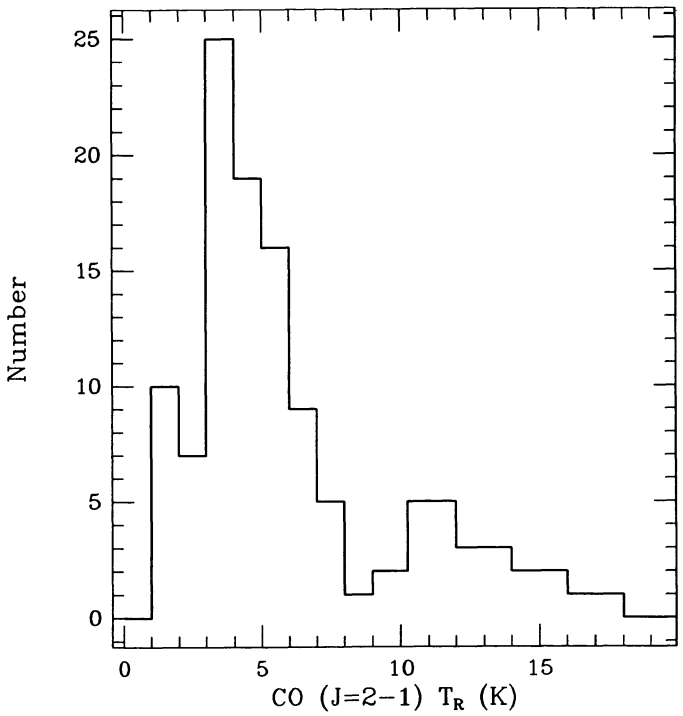

FIG. 12.—MWO sample distribution of corrected CO $J=2$–1 temperatures (T_R) toward 93 of the cataloged clouds. The sample mean is 5.3 K.

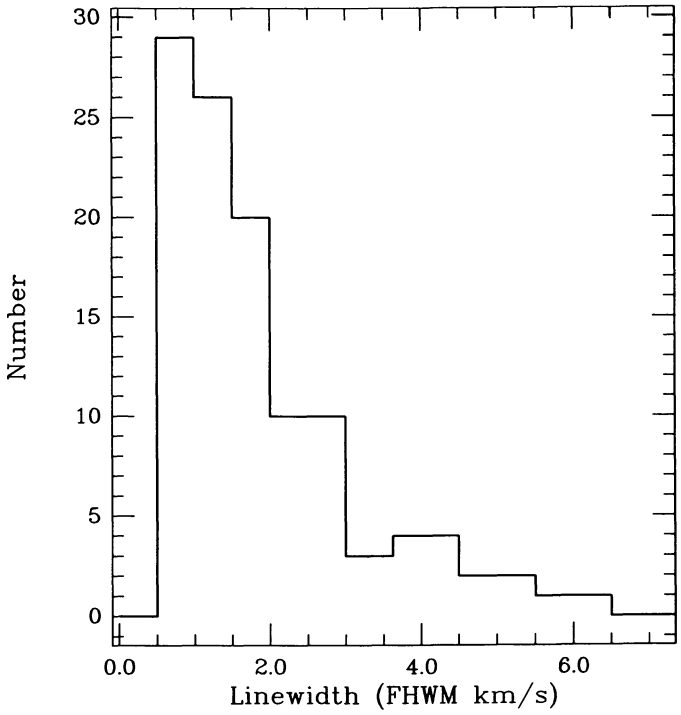

FIG. 13.—MWO sample distribution of CO line widths (FWHM) seen toward 93 of the cataloged clouds.

iii) *The* 100 μm *PSC Flux Distribution*

Figure 11 shows the distribution of observed 100 μm fluxes for the PSC core region detections of clouds in Table 1. The dashed line represents the fit to the upper four flux bins. It gives some indication of the physical nature of the clouds which were *not* detected in the PSC. The PSC is incomplete below 3 Jy at 100 μm, but if it were complete to below 1 Jy *and* the same dashed line were to apply to the lowest flux bin, the expected cloud detection rate should exceed 80%. In fact, this detection rate *is* seen for the co-added *IRAS* survey data (Clemens 1988). More important than the detection rate is the point that these low-luminosity or cold clouds may be the isolated clouds which are *not* forming stars. Finding and studying this sample of inactive clouds is very important, since most of the interstellar gas is inactive. Such a sample would be very different in character from the BM sample, wherein every object is thought to be actively forming stars.

Alternatively, it is possible that the derived slope, -0.69 ± 0.30, is due in part to the flux-limited nature of this sample. For a flux-limited sample of *uniform luminosity* objects, the expected slope is -1.5. Without individual cloud distances, it is difficult to eliminate this possibility.

d) *Millimeter-Wave* CO *Properties*

The MWO ^{12}CO $J=2$–1 survey of 97 of the cataloged clouds forms an interesting data set for uncovering the range of physical conditions sampled by the globules. Figure 12 shows the histogram of corrected peak line temperatures (T_R) for the clouds. The most probable values are in the range of 3–4 K, while the sample mean is somewhat higher at 5.3 K. For optically thick, thermalized CO lines, these brightness temperatures correspond to gas kinetic temperatures of 7.3–8.5 and 9.9 K, respectively. There is a weak secondary peak near 11 K T_R ($\sim$16 K kinetic temperature), which is discussed further below.

Figure 13 shows the distribution of ^{12}CO $J=2$–1 line widths (FWHM) for the MWO sample. Most clouds have line widths smaller than 2 km s^{-1}, and a large number ($\sim$30%) have line widths smaller than 1 km s^{-1}. Corrections due to filter resolution, saturation broadening, and baseline removal conspire to broaden the true gasdynamical line width to the values observed. Hence the true motions of the gas in the clouds with line widths under 1 km s^{-1} are *subsonic* (cf. Dickman and Clemens 1983 for discussion of line broadening in Bok globules). There is also a tail to large line widths, which is discussed below.

Figure 14 presents the distribution of observed line-center velocities for the MWO sample. The sample mean is 6 km s^{-1}, and the dispersion is 10 km s^{-1}. This distribution confirms the local nature of the sample of clouds: all velocities are very near to 0 km s^{-1}. If the dispersion is related to Galactic shear (though the value is only about a factor of 2 greater than that due to random cloud-cloud motions), then for an Oort A constant of 17.7 km s^{-1} kpc^{-1} (Clemens 1985), the mean distance to the clouds is just under 600 pc—very similar to the result found from the latitude distribution.

e) *Comparison of IRAS and Millimeter Results*

The most interesting summary concerning the nature of the MWO sample (and, by extrapolation, the larger, full sample) is contained in Figure 15. There, the derived CO T_R tempera-

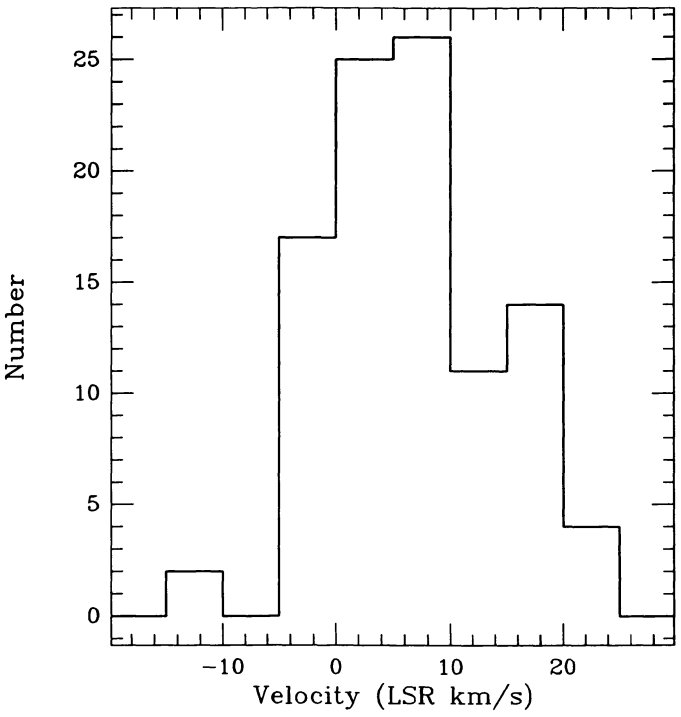

FIG. 14

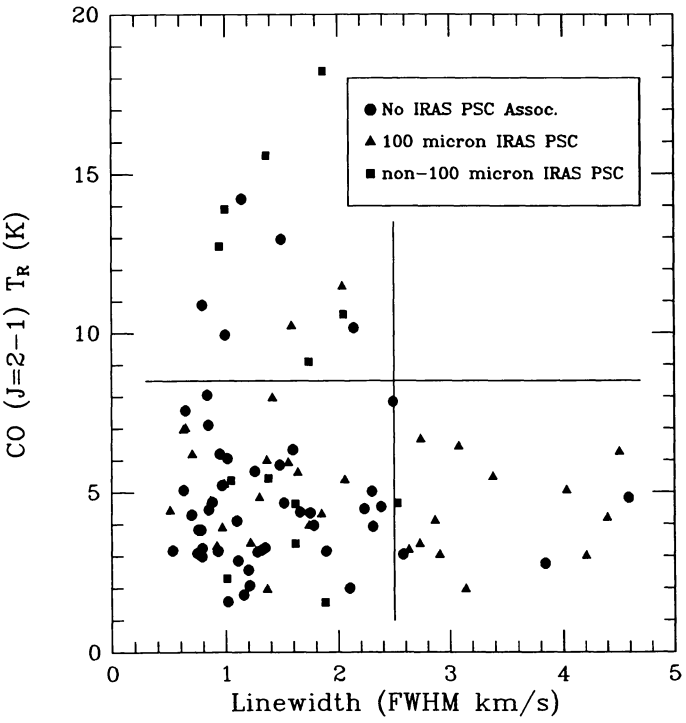

FIG. 15

FIG. 14.—MWO sample distribution of CO line-center velocities seen toward 93 of the cataloged clouds. That the velocities are all very close to 0 km s^{-1} verifies that the sample of clouds is very nearby (~ 600 pc).

FIG. 15.—MWO sample distribution of CO temperatures and line widths for the 93 clouds. As shown in the legend, filled circles indicate clouds with no *IRAS* PSC detections, filled triangles indicate clouds with 100 μm detections (cool sources), and filled squares indicate clouds with shorter wavelength detections (non–100 μm, hence warmer sources). The solid lines at 2.5 km s^{-1} and 8.5 K divide the diagram into four quadrants: hot and dynamically active (*upper right*); hot and quiescent (*upper left*); cold and dynamically active (*lower right*); and cold and quiescent (*lower left*). Note that 70% of the globules are in the lower left quadrant, that the hot clouds have a large number of associated warm *IRAS* sources, and that the cold, dynamically active sample has a preponderance of cool but luminous *IRAS* sources.

tures and line widths are plotted as independent axes. Further, different symbols are used to distinguish the infrared signatures of each cloud. Filled circles indicate clouds which did not have associated *IRAS* PSC core entries and are presumably the coolest or least FIR-bright of the catalog. Clouds containing *IRAS* PSC core sources with 100 μm detections are plotted as filled triangles. These are presumably either warmer or more luminous than the nondetections. Finally, those *IRAS* PSC core detections in the shorter wavelength bands which had *no* detection at 100 μm are plotted as filled squares. These represent the hottest *IRAS* sources.

On the figure, lines at 2.5 km s^{-1} of line width and 8.5 K of CO temperature roughly correspond to breaks in the distributions shown as Figures 12 and 13. These lines divide Figure 15 into four quadrants. First, note that there are no clouds in the upper right quadrant—that corresponding to clouds with warm gas and very supersonic motions. In a similar plot of active H II regions in molecular clouds, this quadrant would be significantly populated as high-mass star formation both heats and stirs up the local molecular gas.

Second, note that the upper left quadrant has six of 13 clouds showing hot *IRAS* sources and two clouds with cooler *IRAS* sources. These warm, but narrow-lined, clouds are therefore likely heated by local, but probably not embedded, stars via radiation, with little of the gasdynamical mixing typically produced by stellar winds.

Third, the lower right quadrant of the figure represents those clouds with unusually large line widths, but no bulk heating of the gas. As the number of cool *IRAS* sources in that quadrant is high (13 of 18), these clouds are likely the sites of embedded protostellar activity. The sources are bright in the FIR, and the gas motions are significantly more energetic than in the quiescent clouds. This subsample of clouds is ideal for studying the effects of protostellar activity on the molecular environment.

Finally, the lower left quadrant contains the vast majority of the clouds (70%). Within this quadrant, the clouds seem to cluster around line widths of about 1 km s^{-1} and temperatures between 3 and 5 K (7 and 9 K kinetic temperature). The cold, quiescent (perhaps subsonic, or only mildly transonic) state is the *preferred* one for these molecular clouds.

Analysis of the quiescent clouds and comparisons with their more active cousins will provide information regarding the physical state of the molecular gas *prior* to star formation. Studying the interrelation between cloud rotation, magnetic fields, and the environments of clouds should allow accurate refinements of star formation models to be made.

V. SUMMARY

A catalog of small, optically selected molecular clouds has been presented. The relevant selection criteria were small angular size (smaller than 10′, mean size of the sample being

4′), large central opacity, and freedom from connecting opaque material. The mean ellipticity of the sample of 248 clouds found on the northern POSS prints was 2.0, with a maximum ellipticity in the sample of 7. The position angle of the clouds was found to be uncorrelated with the direction of the Galactic plane.

A large fraction of the cataloged clouds (60%) had associated *IRAS Point Source Catalog* sources in their cores or envelopes. The likelihood of a detection of a PSC source (per unit area) was some 6.1 times higher for the core regions of the clouds than for the envelopes, indicating a strong association of FIR sources and Bok globules. The associated *IRAS* sources tended to be cooler (~19 K) for the clouds cataloged here than for the embedded cloud cores of BM. The clouds found here showing the smallest 100 μm fluxes are likely not forming stars at this time, and therefore represent an important class of objects for future study.

A sample of 97 of the clouds were observed at the MWO in the $J = 2$–1 line of ^{12}CO. Of this sample, 70% have cold gas kinetic temperatures (~ 8 K) and approximately sonic line widths. The remaining 30% are roughly equally divided between those clouds likely to be radiatively heated by nearby stars and those undergoing active protostellar collapse or outflows with no bulk gas heating.

Note added in manuscript.—A second set of CO $J = 2$–1 observations were made during 1988 March 11–21 at the MWO using the same equipment and technique described above. Over 120 of the cataloged clouds were observed or reobserved under excellent weather conditions. Cloud radial velocities derived from these data have been included in Table 1. Full analysis of the line temperatures and line widths derived from these data has been deferred to a later paper.

Publication of this catalog would have never taken place without the timely delivery of large quantities of guilt by Drs. Bob Dickman and Neal Evans. Both the Five College Radio Astronomy Observatory, University of Massachusetts, and the Millimeter Wave Observatory, University of Texas, are owed a great deal of thanks for awarding our project significant observing time. Dr. Roc Cutri supplied the machine-readable version of the second release of the *IRAS* PSC used in the correlation. Cathy Clemens performed the catalog verification pass on the POSS. Reduction of the spectral line data was performed on the VAX 11/750 operated by the Sub Millimeter Telescope Group at Steward Observatory using the program SPA written and supplied by Dr. N. Scoville. The Five College Radio Astronomy Observatory is operated with support from the National Science Foundation under grant AST 85-12903, and with permission of the Metropolitan District Commission, Commonwealth of Massachusetts. The Millimeter Wave Observatory is operated by the Electrical Engineering Research Laboratory of the University of Texas at Austin with support from the National Science Foundation and McDonald Observatory. This work has been supported by a NASA–IRAS General Investigator grant to D. C. and R. B., and a Cottrell grant from the Research Corporation to D. C.

REFERENCES

Barnard, E. E. 1927, *A Photographic Atlas of Selected Regions of the Milky Way. II. Charts and Tables* (*Carnegie Inst. Washington Pub.*, No. 247).
Beichman, C. A., Myers, P. C., Emerson, J. P., Harris, S., Mathieu, R., Benson, P. J., and Jennings, R. E. 1986, *Ap. J.*, **307**, 337 (BM).
Clemens, D. P. 1985, *Ap. J.*, **295**, 422.
_____. 1988, in preparation.
Clemens, D. P., and Leach, R.W. 1987, *Opt. Engineering*, **26** (No. 9), 923.
Clemens, D. P., Leach, R. W., and Barvainis, R. 1988, in *Molecular Clouds in the Milky Way and External Galaxies*, ed. J. Young, R. Snell, and R. Dickman (New York: Springer-Verlag), in press.
Clemens, D. P., Sanders, D. B., and Scoville, N. Z. 1988, *Ap. J.*, **327**, 139.
Dickman, R. L., and Clemens, D. P. 1983, *Ap. J.*, **271**, 143.
IRAS Catalogs and Atlases, Explanatory Supplement. 1985, ed. C. A. Beichman, G. Neugebauer, H. J. Habing, P. E. Clegg, and T. J. Chester (Washington, DC: GPO).
IRAS Point Source Catalog, 1985, Joint *IRAS* Science Working Group (Washington, DC: GPO) (PSC).
Khavtassi, J. 1955, *Bull. Abastumani Obs.*, **18**, 29.
Lee, M. H., and Rogers, C. 1987, *Ap. J.*, **317**, 197.
Low, F. J., *et al.* 1984, *Ap. J.* (*Letters*), **278**, L19.
Lynds, B. T. 1962, *Ap. J. Suppl.*, **7**, 1.
_____. 1965, *Ap. J. Suppl.*, **12**, 163.
Maddalena, R. J., Morris, M., Moscowitz, J., and Thaddeus, P. 1986, *Ap. J.*, **303**, 375.
Magnani, L., Blitz, L., and Mundy, L. 1985, *Ap. J.*, **295**, 402.
Schoenberg, E. 1964, *Bayerische Akad. Wiss.* **5** (No. 26), 5.
Ungerechts, H., and Thaddeus, P. 1987, *Ap. J. Suppl.*, **63**, 645.

RICHARD BARVAINIS: Haystack Observatory, NEROC, Route 40, Westford, MA 01886

DAN P. CLEMENS: Department of Astronomy, Boston University, 725 Commonwealth Avenue, Boston, MA 02215